Global and Planetary Change 219 (2022) 103978

Contents lists available at ScienceDirect

Global and Planetary Change

journal homepage: www.elsevier.com/locate/gloplacha

How does seismic attenuation correlate to rheology of crustal rocks? Results from a numerical approach

Maria Aurora Natale Castillo [a], Magdala Tesauro [a,b,*], Mauro Cacace [c]

[a] University of Trieste, Department of Mathematics and Geosciences, Trieste, Italy
[b] Department of Earth Sciences, Utrecht University, Utrecht, Netherlands
[c] German Research Centre for Geosciences (GFZ) Potsdam, Germany

ARTICLE INFO

Editor: Zhengtang Guo

Keywords:
Rocks rheology
Seismic attenuation
Strength envelopes
Burgers model
Gassmann model

ABSTRACT

Most natural resources are distributed within the uppermost layer of the lithosphere and their exploitation is limited by the transition from brittle to ductile rocks' deformation (BDT), which coincides with a strong reduction in rocks permeability. Therefore, knowledge of the physical and mechanical crustal properties is crucial for improving our understanding of the exploitable potential. Previous studies have showcased the existence of a relation between rocks' seismic attenuation and their viscous modes of deformations, considering that both depend on intrinsic rocks characteristics (e.g., grain size, fluid content) and background P-T conditions.

In this study, we investigate such quantitative relationships between seismic attenuation and viscous rocks' rheology across the domain where rocks transition from a dominant brittle to a more ductile deformation mode. We rely on the Burgers and Gassmann mechanical model to derive shear wave attenuation ($1/Q_s$), for several dry and wet crustal rheology, thermal conditions, and different strain rates. This allows us to establish geothermal and mechanical conditions at which the BDT occurs and cross-correlate this transition to computed shear seismic wave attenuation values. In particular, we observe that Q_s variation with depth is more sensitive to the input strain rate than to the adopted rock's rheology and thermal conditions, so that a fixed amount of the Q_s reduction can be used to identify the average BDT depths for each strain rate used. Below the BDT depth, we observe a significant drop in Q_s (up to 10^{-4} % of the surface value), being also influenced by the background temperature and rock rheology. Since the greatest Q_s reduction is estimated for the highest input strain rate (10^{-13} s^{-1}), our results have implications for tectonically active/geothermal areas. Ongoing and future works will focus on a further validation of the modelling implications by systematic analyses of observations derived from rocks' laboratory experiments. The last ones can add constraints on the relationship found in this study between seismic attenuation and adopted rheological flow law.

1. Introduction

The crust, the outer shell of the Earth, is characterized by strong thermo-physical heterogeneities, due to lateral and depth variations in the the structure and composition of the rocks. This layer is in direct contact with the atmosphere and surface waters, whose dynamics, together with tectonic stresses, produce such major structural changes and control the presence and distribution of available natural resources (e.g., water, oil, gas). In addition, long-lived radioisotopes ^{238}U, ^{235}U, ^{232}Th, and ^{40}K, are mainly concentrated in the crust, in particular in its sialic part. There, thermal anomalies, which are responsible for the formation of geothermal resources, can be also caused by the presence of magma bodies. Exploration and exploitation of natural resources require a proper understanding of the mechanical crustal properties. These properties are described by rocks strength variations within a specific geodynamic context (Burov, 2011). Indeed, crustal rocks can deform preferentially either in a brittle or ductile mode and the yield strength envelope (YSE) provides the maximum rock strength given by the minimum of the two mechanisms of deformation (Goetze and Evans, 1979). The first-order rheological behaviour (brittle or ductile), at any given depth, is determined by the relative magnitude of frictional (brittle) and creep (ductile) strength. If the critical stress difference for frictional sliding is less than the creep strength, failure by frictional sliding will predominate, while in the opposite case, ductile flow will

* Corresponding author at: University of Trieste, Department of Mathematics and Geosciences, Trieste, Italy.
E-mail address: mtesauro@units.it (M. Tesauro).

https://doi.org/10.1016/j.gloplacha.2022.103978
Received 23 March 2022; Received in revised form 4 September 2022; Accepted 19 October 2022
Available online 27 October 2022

occur (e.g., Ranalli and Murphy, 1987). According to Karato (2008), brittle deformation involves cracks formation and deformation of the pores of the rocks (cataclastic deformation), while ductile deformation concerns rocks point defects, dislocations, and grain boundaries (crystal plasticity). The depth of the transition from the brittle to ductile deformation (BDT) commonly refers to a pressure and temperature range, where rocks deform by an interplay of cracking and crystal plasticity, marking the progressive change in crustal rheology with increasing depth (Meyer et al., 2019). This transition occurs at a variable depth, depending on the rock's structure, composition, hydrous conditions, and amount and type (compression or extension) of tectonic stress (e.g., Burov, 2011). Therefore, the interplay of the Earth's physical conditions (i.e. *P*,*T* conditions) and rocks physical characteristics determine, to a first order, the crustal mechanical behaviour. Indeed, the temperature at which the crust can start to flow, T_{BDT} (BDT temperature), depends on its silica content and it usually occurs at about 380–400 °C in rhyolites/granites rocks and at 500–600 °C in basalts/gabbros (e.g., Elders et al., 2014). The T_{BDT} exerts a key control on the formation of supercritical fluids (e.g., Scott et al., 2015). Indeed, the water enthalpy in conventional high enthalpy geothermal systems depends strongly on rock permeability (e.g., Norton and Knight, 1977; Driesner and Geiger, 2007), which markedly decreases at the depth of the BDT. The BDT occurs at depths of 10–15 km in typical crustal rocks, subjected to regional metamorphic geotherms, or at shallower depth levels in areas of active magmatism (Watanabe et al., 2017). Therefore, drilling procedures for the exploitation of supercritical geothermal resources for power production requires a rigorous understanding of how rocks physical parameters influence the bulk behaviour of crustal rocks. Depicting the mechanical rocks behaviour is crucial to best plan exploitation of supercritical fluids, as well as to assess the economic potential of these deep geothermal reservoirs and other natural resources (e.g., Violay et al., 2017). The BDT approximately occurs at the depth above 95% of intraplate earthquakes are generated and thus it also provides a conservative estimate of the thickness of the crustal seismogenic layer (e.g., Burov, 2011). Therefore, understanding of the mechanical rocks properties has also implications for a proper assessment of the seismic hazard, especially in tectonically active areas.

The mechanical behaviour of rocks, and in particular their transition from a brittle to a ductile deformation, has been extensively investigated through a vast amount of rheological experiments (see Burgmann and Dresen, 2008 for a review), numerical models (e.g., Burov, 2011; Jacquey and Cacace, 2020), and seismicity studies (e.g., Maggi et al., 2000; Jackson, 2002). In this respect, the analyses of seismic wave propagation in high-enthalpy geothermal regions, in the presence of (partial) melting can improve our knowledge of physical rocks behaviour and provide an alternative assessment of the BDT (e.g., Cermak et al., 1990; Vinciguerra et al., 2006; Kristinsdóttir et al., 2010; Carcione and Poletto, 2013; Poletto et al., 2018). Indeed, viscous rocks deformation, depending on the rock structure, composition, and fluid content, as well as on the in-situ T-P conditions, can be analysed through the study of seismic attenuation, defined as the dissipation of seismic energy as it propagates through the rock medium. Seismic attenuation is usually described in terms of a "quality factor" *Q*, given by the inverse of the fractional loss of energy per wave cycle. Therefore, the estimation of the seismic quality factor (*Q*) can be used to quantify the energy loss of seismic waves, which provides an indirect measure of the anelastic behaviour of the Earth's materials. The *Q*-factor is a function of the dynamic mechanical response of a system (i.e. natural rock samples, Cooper, 2002), and it depends on the seismic frequency, as well as on the temperature, water content, and grain size of the rocks (e.g., Karato and Spetzler, 1990; Karato, 1993; Jackson and Faul, 2010). It can be mathematically described by an Arrehenius-type equation, in a similar fashion to the viscous rocks deformation (Cammarano et al., 2003). Despite previous studies have discussed the existence of a correlation between the seismic attenuation and onset of viscous deformation in rocks, the sensitivity of this quantitative relationship to background tectono-thermal conditions and varying rock's physical properties have been not yet properly investigated.

Some recent studies (e.g., Carcione and Poletto, 2013; Poletto et al., 2018; Farina et al., 2019) computed seismic wave properties, relying on the Burgers mechanical model (Fig. 1). This model, which provides the most anelastic model, is described by a combination in series of a Zener and Maxwell model, being characterized by two (short- and long-term) viscosities (Karato, 2008). According to Carcione and Poletto (2013), the Burgers model provides the most reliable description of the behaviour of ductile media, since is able to capture both transient and steady-state (secondary) creep in a consistent way. These previous studies coupled the Burgers model with a modified Gassmann model to account for the additional effect of fluids saturating the porous rocks. As an example, Jaya et al. (2010), based on the analyses of petrophysical experiments on Icelandic geothermal rock samples at simulated in situ reservoir conditions, relied on a modified Gassmann model to quantify the effect of varying temperature conditions on seismic velocity and attenuation, with the aim to predict the secondary role of pore fluid on these variations. More recently, Farina et al. (2019), computed seismic velocities and their attenuation, relying on the combined Burgers and Gassmann model, with the aim of characterizing the geothermal resources at the "Los Humeros" supercritical geothermal field in Mexico. Seismic parameters were computed at the mesoscale (i.e. scale of the whole reservoir), considering the depth distribution of temperature, as well as confining and pore pressure variations encountered in the field. Viscous rock's deformation was accounted for via a dislocation creep equation, relating differential stress to imposed strain rate values.

Following the numerical approach proposed by Farina et al. (2019) and other previous studies (e.g., Carcione and Poletto, 2013; Poletto et al., 2018), we compute the seismic quality factors for shear waves (Q_s) for a wide range of geological and tectono-thermal settings, in terms of the chosen rheological prototypes, strain rates, and geotherms. We further compare the obtained Q_s depth variations with variations in shear viscosities and computed ductile strengths profiles. To this purpose, we chose two sialic rocks (granite and quartzite), under hydrated and anhydrous conditions and three mafic rocks (diabase, OPX and CPX), under anhydrous conditions only. In addition, we compute strength envelopes for all crustal rocks, temperature, and strain rate conditions. The comparison of the obtained results enables us to quantify the sensitivity of the seismic attenuation and strength distribution on the input parameters and therefore to describe in a quantitative manner the correlation between the computed Q_s reduction (i.e. seismic attenuation increase) and depth, as induced by the resolved ductile deformation.

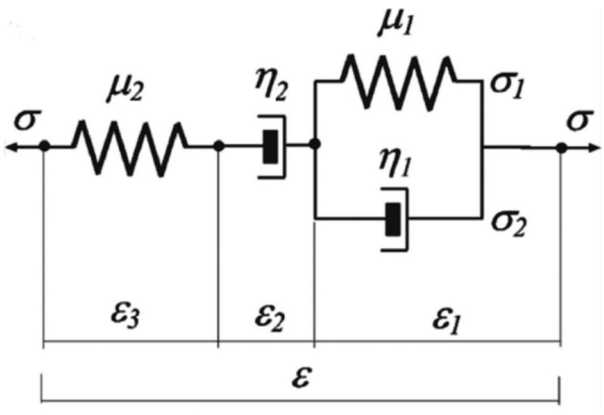

Fig. 1. Burgers mechanical model. σ, ε, μ, and η represent stress, strain, shear modulus, and viscosity, respectively, where σ_1, ε_1, and η_1 refer to seismic relaxation or retarded behaviour (Zener model), while σ_2, ε_2, and η_2 refer to plastic flow and viscous deformation (Burgers model).

2. Method

Below, we describe how the main thermophysical rocks' parameters have been obtained. A table with the names of the variables, units and range of values is provided in Appendix A1.

2.1. Shear modulus (μ)

As in previous studies (e.g., Farina et al., 2019; Carcione and Poletto, 2013; Carcione et al., 2014), we estimate the Q_s through the frequency dependent shear modulus of the rock, according to the Burgers mechanical model (1):

$$\mu_B = \frac{\mu_o(1 + i\omega\tau_\epsilon)}{1 + i\omega\tau_\sigma - \frac{i\mu_o}{\omega\eta_s}(1 + i\omega\tau_\epsilon)} \quad (1)$$

$$i = \sqrt{(-1)} \quad (2)$$

Where μ_B is the Burgers shear modulus, μ_o the dry shear modulus of the rock at ambient P, T conditions, ω the angular frequency, i the imaginary part (2), η_s the shear viscosity (hereafter, we refer to it as viscosity), τ_σ and τ_ϵ are the seismic relaxation times, which can be expressed as:

$$\tau_\epsilon = \frac{\tau_0}{Q_0}\left(\sqrt{Q_0^2 + 1} + 1\right) \quad (3)$$

$$\tau_\sigma = \tau_\epsilon - \frac{2\tau_0}{Q_0} \quad (4)$$

In (3) and (4) Q_0 is the minimum quality factor and τ_0 a relaxation time, such that $\omega_0 = 1/\tau_0$ is the center frequency of the relaxation peak (Farina et al., 2019). As in Farina et al. (2019), τ_0 is computed using $Q_0 = 122$ for a seismic frequency $f = 3$ Hz. This Q_0value is representative of southern Italy upper crust (Castro et al., 2008), where the approximated frequency dependence relationship for that area is:

$$Q_0 = 18.8f^{1.7} \quad (5)$$

with $f < 100$ Hz. Several previous studies (e.g., Sato et al., 2012) predict for volcanic areas lower values of Q_0 and of the exponent in the frequency dependence relationship. However, we prefer to keep those used in Farina et al. (2019), since they are likely to be applicable to wider thermophysical conditions, considering the heterogeneous nature of the upper crust of southern Italy.

The values of μ_o for the sialic rocks (granite and quartzite) and diabase are assumed equal to that of the granite sample described in Farina et al. (2019). Indeed, the shear modulus at ambient conditions of these rocks span a similar range (e.g., Turcotte and Schubert, 2014; Mavko et al., 2010) and the assumed value lies within this range. In contrast, the values of μ_o of the OPX and CPX are taken from Cammarano et al. (2003), being greater than those of the other rocks. Indeed, the OPX and CPX are principal constituents of upper mantle rocks, though they are also present in variable portions in the crust.

2.2. Shear viscosity (η_s)

The η_s, is obtained by modelling viscous flow of the rocks, according to a power-law creep (Goetze and Evans, 1979), computed for the seven different rocks rheologies (Table 1):

$$\sigma_D = \left[\frac{\dot{\varepsilon}}{A_{PL}}\right]^{\frac{1}{N}} . exp\left[\frac{E_{PL}}{NRT}\right] \quad (6)$$

where σ_D is the differential stress, $\dot{\varepsilon}$ the strain rate, A_{PL} the pre-exponential factor, E_{PL} activation energy, N the exponential factor, R the gas constant (8.314 J/mol/K), and T the absolute temperature. We compute the differential stress using two different geotherms and three fixed values of strain rate (10^{-13} s^{-1}, 10^{-15} s^{-1}, and 10^{-17} s^{-1}, respectively), consistent with global estimates, based on horizontal geodetic velocities (Kreemer et al., 2014).

Table 1
Values of the physical parameters of hydrous (wet) and anhydrous (dry) rocks chosen in this study. Values of the power law creep parameters (A_{PL}, E_{PL}, and N) are taken from Carter and Tsenn (1987), grain densities at ambient P,T conditions (ρ_s) from (1) Christensen and Mooney (1995) and (2) Cammarano et al. (2003), and shear modulus at ambient P,T conditions (μ_0) from (1) Farina et al. (2019) and (2) Cammarano et al. (2003).

Lithology	A_{PL} [$Pa^{-N}s^{-1}$]	E_{PL} [J/mol]	N	ρ_s [kg/m^3]	μ_o [GPa]
Dry Granite	3.16E^{-26}	186,500	3.3	2682.0$^{(1)}$	37$^{(1)}$
Wet Granite	7.94E^{-16}	140,600	1.9	2682.0$^{(1)}$	37$^{(1)}$
Dry Quartzite	6.03E^{-24}	134,000	2.72	2672.8$^{(1)}$	37$^{(1)}$
Wet Quartzite	1.26E^{-13}	172,600	1.9	2672.8$^{(1)}$	37$^{(1)}$
Dry Diabase	3.16E^{-20}	276,000	3.05	2964.8$^{(1)}$	37$^{(1)}$
Dry OPX	1.26E^{-15}	293,000	2.4	3215$^{(2)}$	75$^{(2)}$
Dry CPX	1.58E^{-37}	380,000	5.3	3277$^{(2)}$	67$^{(2)}$

The η_s is then computed as an effective viscosity (η_{eff}), considering the relationship between the deviatoric stress (σ_{II}) and strain rate ($\dot{\varepsilon}_{II}$) invariants:

$$\eta_{eff} = \frac{\sigma_{II}}{2\dot{\varepsilon}_{II}} \quad (7)$$

The reformulation (8,9) is based on the type of the rheological experiments, axial compression in the cases considered (Gerya, 2019):

$$\sigma_D = \sqrt{3}\sigma_{II} \quad (8)$$

$$\eta_{eff} = \frac{1}{3^{(N+1)/2}} \times \frac{1}{A_{PL}(\sigma_{II})^{(N-1)}} exp\left(\frac{E_{PL}}{RT}\right) \quad (9)$$

The two geotherms, reflecting the possible thermal conditions of an old tectonically stable (intracratonic) and young, recently (re)activated area, are computed with a resolution of 1 km up to a depth of 40 km, following the iterative method of Hasterok and Chapman (2011):

$$T_{i+1} = T_i + \frac{q_i}{k_i}\Delta z_i - \frac{A_i}{2k_i}\Delta z_i^2 \quad (10)$$

$$q_{i+1} = q_i - A_i\Delta z_i \quad (11)$$

where the temperature and heat flow values at the bottom of each layer of the thickness Δz_i (T_{i+1}, and q_{i+1}, respectively) are determined from those at the top (T_i, and q_i), while A_i and k_i are the radiogenic heat and thermal conductivity of each layer. We use surface heat flow (*SHF*) values of 50 mWm^{-2} and 80 mWm^{-2}, which can be considered as representative of the two end-member tectonic conditions. We assume a linear decrease in the concentration of the radiogenic heat from the surface to the bottom of the crust (e.g., Hasterok and Chapman, 2011) and defined two ranges of values, (i) between 2.1 and 0.1 μWm^{-3}, associated to the *SHF* 50 mWm^{-2} and (ii) between 3.0 and 0.2 μWm^{-3}, associated to the *SHF* 80 mWm^{-2}. The thermal conductivity is assumed to linearly increase with depth and we define a range between 1.5 and 3.5 Wm^{-1} K^{-1}, considering that sialic rocks have on average a thermal conductivity lower than ultramafic rocks (e.g., Goes et al., 2020). The two geotherms displayed in Fig. 2 (referred to '*warm*' and '*cold*' geotherm hereafter) displays a decrease in thermal gradients with depth, reflecting the decrease in the concentration of radiogenic heat input. The temperature at the base of the crust is about 730 °C and 415 °C, for the '*warm*' and '*cold*' geotherm, respectively, consistent with the values derived from global models (e.g., Artemieva, 2006).

2.3. Shear seismic quality factor (Q_S)

According to Farina et al. (2019), we use the Burgers mechanical model augmented with the Gassmann model to describe the effects of

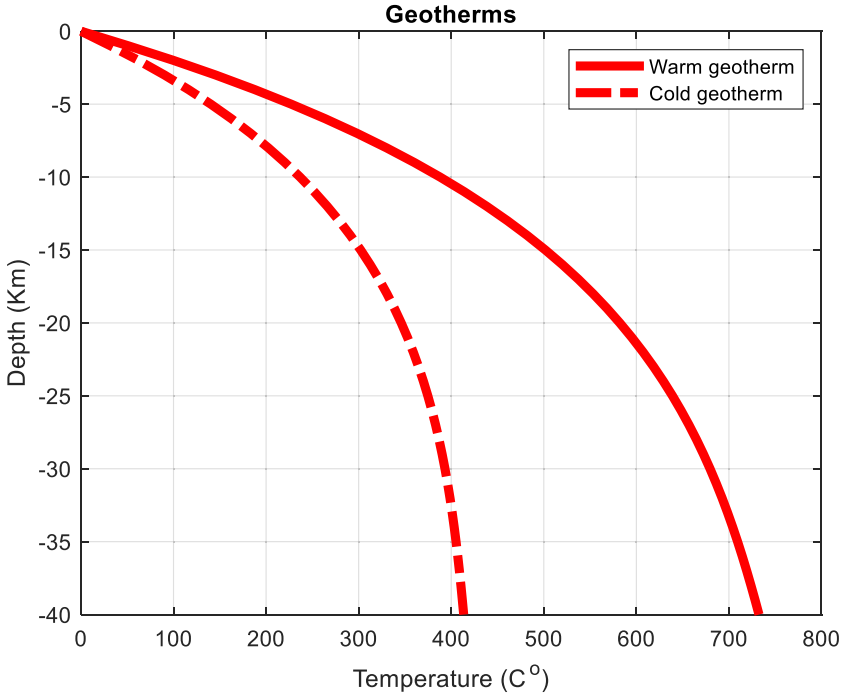

Fig. 2. Temperature depth distribution for the "*warm*" and "*cold*" geotherms. See main text for further explanations.

seismic wave's amplitude loss in wet and dry crustal rocks rheology, respectively. Within this theoretical framework, the frequency dependent shear modulus provides the link to the viscolastic media into the Gassmann equations for a poroelastic media. According to the Gassmann model, the saturated-rock shear modulus is given by $\mu_G = \mu_m$, where μ_G stands for the dry-rock Gassmann shear modulus and μ_m is the dry-rock shear modulus, which depends on pressure (e.g., Carcione, 2014). Since the dry rock's composition is assumed to be the same as of that of a granular material (e.g., Farina et al., 2019), the elastic behaviour of these aggregates displays a non-linear dependency on pressure, which can be expressed as in Kaselow and Shapiro (2004):

$$\mu_m(p_d) = \mu_B.[1 - (1 - a_2).exp(-p_d/p_2)] \tag{12}$$

where μ_B (1) is equal to μ_0, at infinite high confining pressure (Table 1), a_2 and $p_2$are constant (equal to 0.48 and 55.55, respectively), and p_d is the differential pressure ($p_d = p_c - p_o$), with p_o and p_c the pore and confining pressure, respectively. We assume p_0 equal to 36% of p_c (consistent with hydrostatic conditions) for wet rheologies and to zero for dry rheologies, while we compute p_c as the product of $\rho_w gz$, with ρ_w the bulk density, g the gravity acceleration, and z the depth. ρ_w is computed as a weight average of the grains (ρ_s) and fluid (water or air) density (ρ_f):

$$\rho_w = (1 - \phi)\rho_s + \phi\rho_f \tag{13}$$

The values of ρ_s are taken from Christensen and Mooney (1995) and Cammarano et al. (2003) (Table 1), while ρ_f is assumed equal to 1000 kg/m^3 (for wet rheologies) and 1.225 kg/m^3 (for dry rheologies). We also assume for all rocks a constant porosity value (0.3%) equal to that of one of the granite samples of the study of Farina et al. (2019).

The shear complex velocity is then computed as:

$$V_S(\omega) = \sqrt{\frac{\mu_G(\omega)}{\rho_w}} \tag{14}$$

Since the viscoelastic modulus (and the viscoelastic compliance) of the system is a complex number, it can be demonstrated that the attenuation expressed as Q^{-1}, is equal to the ratio between the imaginary and real component of the modulus, named the "loss modulus" and "storage modulus", respectively (e.g., Findley et al., 1976; Cooper, 2002). The ratio between the real and imaginary part of the squared shear complex velocities gives the shear seismic quality factor as:

$$Q_S = \frac{Re(v^2_S)}{Im(v^2_S)} \tag{15}$$

The seismic attenuation here retrieved is the one related to the total seismic attenuation that a unidimensional wave propagating in a viscoelastic media can exhibit (Carcione, 2015). Further details about the mathematical analysis describing the relationship between the Q_s and V_s are described in Bourbiè et al. (1987) and Carcione (2014).

2.4. Yield Strength Envelopes (YSE)

As discussed in the Introduction section, the YSE represents the minimum stress (brittle or ductile) that a rock can undertake before deforming permanently.

We compute the YSE, for all the tested rheologies and assumed temperature and strain rate values, by using the Byerlee's law (Byerlee, 1978) to approximate brittle conditions:

$$\sigma_b = \alpha\rho_w gz(1 - \lambda) \tag{16}$$

where σ_b is the friction-related differential stress, α a dimensionless parameter, depending on the cohesion, friction coefficient, and orientation of the stress field, and λ the pore fluid factor, defined as the ratio between the pore and confining pressure (p_0/p_c). We use a value of α equal to 0.75 and 3 for extensional (normal faulting) and compressional (reverse faulting) tectonics, respectively (Sibson, 1974), and of λ equal to 0.36, consistent with hydrostatic conditions. The ductile deformation (σ_d) is estimated from the power-law dislocation creep, as in (6) (Table 1).

3. Results

The yield strength envelopes for the seven selected rheologies, together with computed depth variations of the η_s, Q_s, and Q_s reduction are displayed in Figs. 3–16. The Q_s reduction has been computed as the

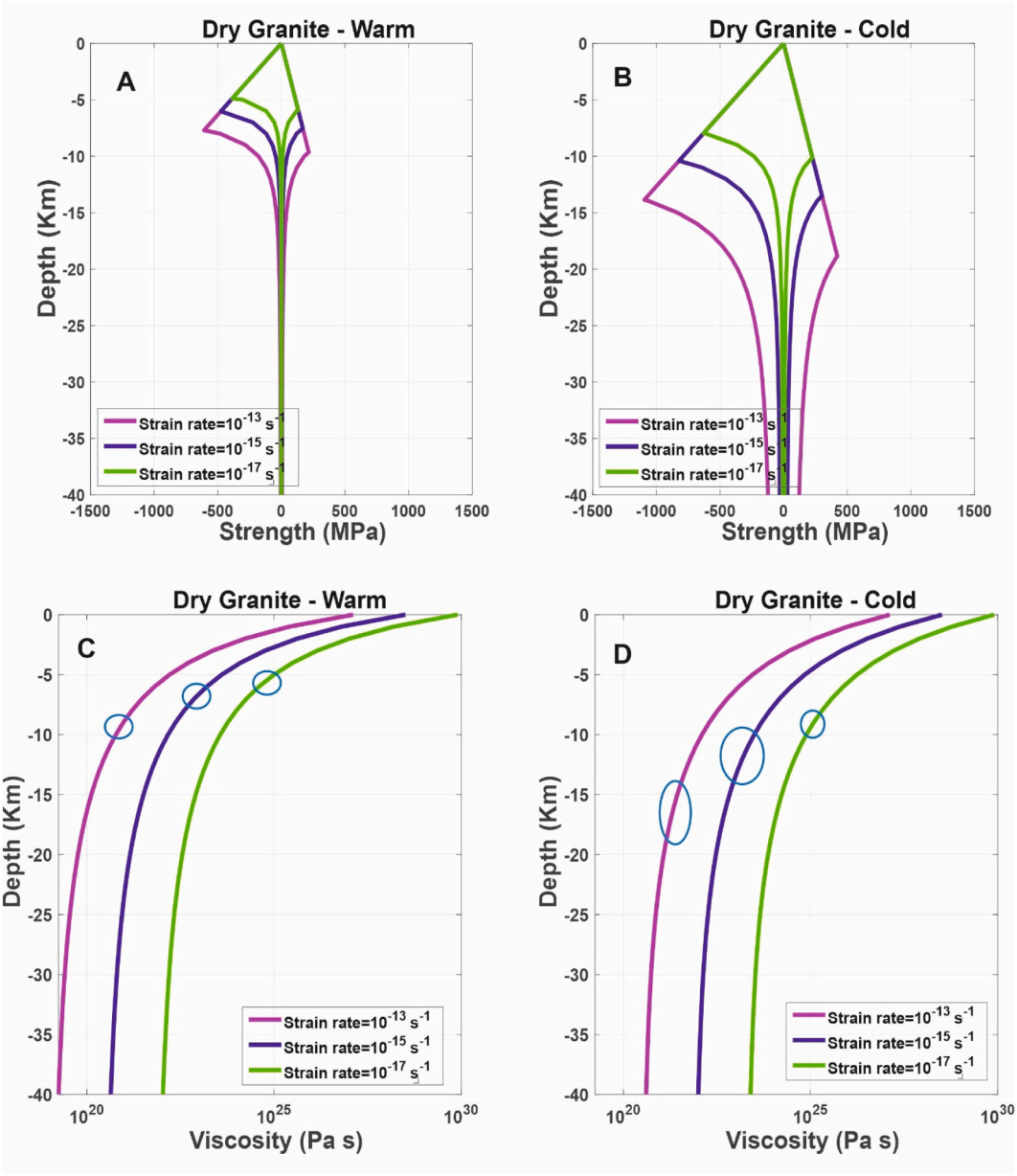

Fig. 3. Results of the numerical tests on dry granite rheology: **(A-B)** strength (MPa) and **(C–D)** viscosity (Pa s) variation with depth, using three different values of strain rate and the **(A** and **C)** '*warm*' and **(B** and **D)** '*cold*' geotherm as input parameters. Light blue ellipses show the range of the BDT depth. See main text for further explanations. (For interpretation of the references to colour in this figure legend, the reader is referred to the web version of this article.)

percentage of the complementary of the ratio between the Q_s value, obtained at each depth, and the maximum value of the Q_s at the surface. Furthermore, we compute the mean of the Q_s and η_s, between values obtained at the depth of the BDT for each strength envelope and display them together with the corresponding T_{BDT} in Table 2. In the following sections, we discuss the results in terms of the strength, η_s, and Q_s reduction variations, without referring directly to the computed Q_s values.

3.1. Sialic rocks

3.1.1. Dry granite

The comparison between the strength envelopes displayed in Fig. 3 A–B reveals how background thermal conditions extert a significant influence on the strength distribution. Maxima in the rock's strength are reached at the BDT depths and are found to vary between 500 and 1000 MPa (Fig. 3A–B), for a given strain rate of 10^{-13} s^{-1}. In addition, the BDT depth varies from 5 to 10 km (using the '*warm*' geotherm) and from 8 to 19 km (using the '*cold*' geotherm) (Fig. 3A–b, Table 2), while the range of the BDT depths for each strength envelope is between 1 and 2 km (using the '*warm*' geotherm) and 2–5 km (using the '*cold*' geotherm), depending on the adopted strain rate (Table 2). We also note that for the '*cold*' geotherm and highest strain rate, the difference in the BDT depth, due to the tectonic regime considered, is enhanced, while it is reduced with an increase in temperature and a decrease in strain rate. We can further observe that the temperature at which the '*warm*' and '*cold*' geotherms intersect the BDT depths varies in a range, between ~35 °C and ~ 60 °C, respectively (Table 2). The mean values of the η_s at the depths of the BDT are within the same orders of magnitude for the two geotherms, for an imposed strain rate of 10^{-13} and 10^{-15} s^{-1}, while considering the minimum value of strain rate results in one order of magnitude difference in the η_s (Fig. 3C–D and Table 2). On the other hand, the mean values of the Q_s reduction, corresponding to the BDT depths are within the same orders of magnitude for the two geotherms

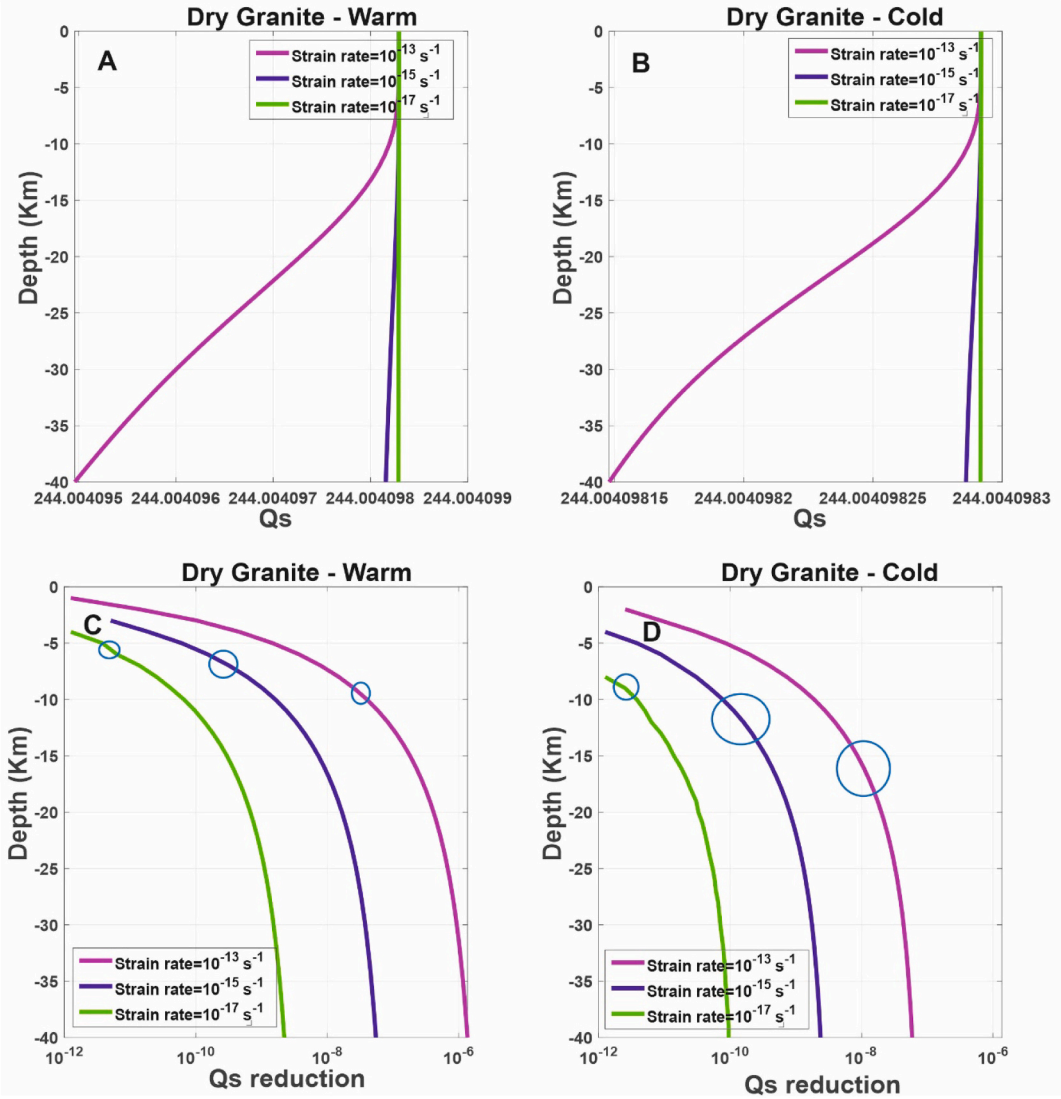

Fig. 4. Results of the numerical tests on dry granite rheology: **(A-B)** Q_s and **(C-D)** Q_s reduction (%) variation with depth, using three different values of strain rate and the **(A** and **C)** '*warm*' and **(B** and **D**) '*cold*' geotherm as input parameters. Light blue ellipses show the range of the BDT depth. See main text for further explanations. (For interpretation of the references to colour in this figure legend, the reader is referred to the web version of this article.)

and for all strain rate values adopted (10^{-8}, 10^{-10}, and10^{-12}%, for strain rate of 10^{-13}, 10^{-15}, and 10^{-17} s^{-1}, respectively).

Below the BDT depth, the strength significantly reduces, reaching negligible values (< 10 MPa) at a depth of 25 km for the '*warm*' geotherm. However, when we use the '*cold*' geotherm, the strength remains above the minimum value of 10 MPa, at the base of the crust, for an input strain rate of 10^{-13} s^{-1}. The decrease in the ductile strength with depth results in a reduction in the η_s at the base of the crust up to a minimum of 10^{19}–10^{22} and 10^{20}–10^{23} Pa s for the '*warm*' and '*cold*' geotherm, respectively. These values correspond to a range of the Q_s reduction between 10^{-6}–10^{-9} and 10^{-8} -10^{-10}%, respectively. We can further notice that the values of the Q_s reduction remain almost constant in the first kilometers of the crust. Indeed, the Q_s starts to reduce at depths 1–4 km and 2–8 km, for the '*warm*' and '*cold*' geotherm scenario respectively (Figs. 4C-D). Therefore, the starting depth at which the Q_s reduction is detectable increases with decreasing temperature and strain rate (Figs. 4C-D).

3.1.2. *Wet granite*

The strength envelopes for a granite rheology under hydrous conditions show a lower amount of strength than for a dry granite (Figs. 5A-B). The maximum value at the BDT depth is about 500 MPa, using as input the '*cold*' geotherm and highest strain rate (Fig. 5B). The maximum BDT depth associated to the highest strain rate value and extensional tectonic conditions occurs at a depth of 6 and 12 km, for the '*warm*' and '*cold*' geotherm, respectively (Table 2). The range of the BDT depth for each strength envelope, depending on the geotherm used, is also reduced, compared to the previous rheology, being within 1 or 2 km (Table 2). We note a similar trend also for the range of T_{BDT} (~35–30 °C). We can further observe that the mean η_s, values at the BDT depths are approximately one order of magnitude lower than those obtained from a dry granite rheology (Figs. 5C-D and Table 2). In contrast, the mean Q_s values are of the same orders of magnitude as for the previous rheology (Figs. 6C-D), except when we use the '*cold*' geotherm and a strain rate of 10^{-17} s^{-1}, for which we observe one order of magnitude increase (Fig. 6D).

Below the BDT depths, the strength reduces to <10 MPa at a depth of about 10 and 25 km, for the '*warm*' and '*cold*' geotherm, respectively, and the maximum strain rate value considered. Furthermore, the η_s significantly decreases, reaching at the base of the crust values in the range of 10^{17}–10^{19} Pa s and 10^{19}–10^{21} Pa s for the two input geotherms (Figs. 5 A-B). At the same depth, the values of the Q_s reduction increase,

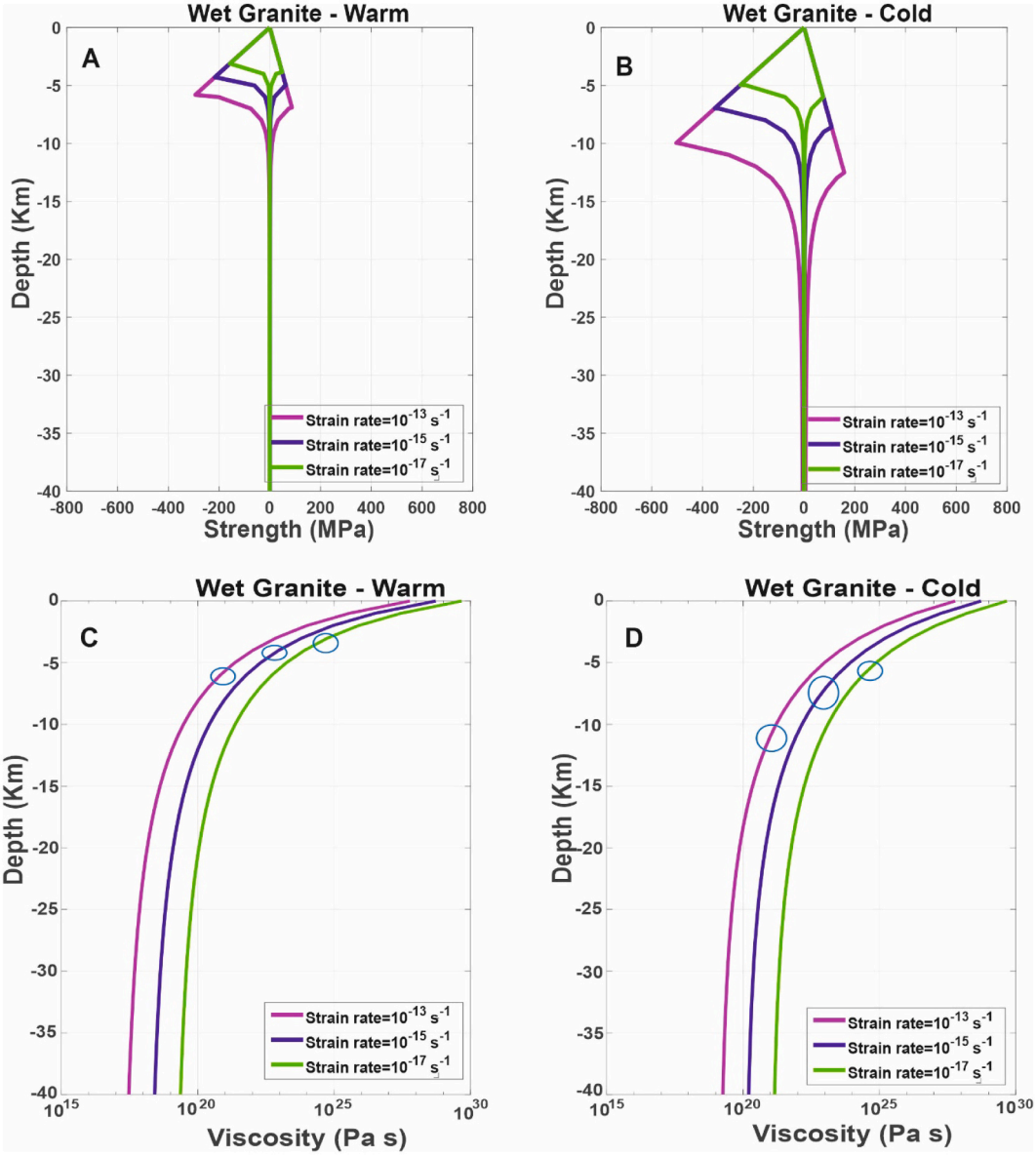

Fig. 5. Results of the numerical tests on wet granite rheology: **(A-B)** strength (MPa) and **(C–D)** viscosity (Pa s) variation with depth, using three different values of strain rate and the **(A** and **C)** '*warm*' and **(B** and **D)** '*cold*' geotherm as input parameters. Light blue ellipses show the range of the BDT depth. See main text for further explanations. (For interpretation of the references to colour in this figure legend, the reader is referred to the web version of this article.)

reaching a range of 10^{-4}–10^{-6}% and 10^{-6}–10^{-8}%, respectively. We can further notice that the *Qs* starts to reduce with respect to its surface value at a shallower depth than for the case of a dry granite rheology (Figs. 6C-D).

3.1.3. *Dry quartzite*

The strength envelopes show shapes, maximum strength values, and BDT depths similar to those of the wet granite rheology (Figs. 7A-B, Table 2). In contrast, with respect to the dry granite rheology, they display a shallower BDT depth, occurring in a range of 1–2 km, corresponding to a temperatures range of ~30–35 °C. At the BDT depth, the mean η_s is one order of magnitude lower when the '*warm*' geotherm and strain rate values of 10^{-13} s^{-1} and 10^{-15} s^{-1} are used, as well as for the case of the '*cold*' geotherm and a strain rate value of 10^{-13} s^{-1} (Figs. 7C-D). On the other hand, the mean Q_s reduction has the same orders of magnitude of the previous rheologies, with the highest value, associated to the greatest strain rate, while reduction in the Q_s starts at depths similar to those of the wet granite rheology (Figs. 8C-D).

Below the BDT depths, when we use the '*warm*' geotherm as input, the strength is reduced to values <10 MPa at a depth between 10 and 15 km, depending on the input strain rate (Fig. 7A). In contrast, for the '*cold*' geotherm, the strength decreases to <10 MPa between 15 and 25 km for strain rate values of 10^{-17} s^{-1} and 10^{-15} s^{-1}, respectively, while remains always above the reference threshold, for the greatest value of strain rate (Fig. 7B). Furthermore, the decrease in the η_s at the base of the crust is significantly reduced compared to the the wet granite rheology, reaching values between 10^{19} and 10^{21} and 10^{20}–10^{22} Pa s, when the '*warm*' and '*cold*' geotherm is used, respectively (Figs. 7C-D). At the same depth and thermal conditions, the Q_s reduction increases up to 10^{-6}–10^{-8} and 10^{-7}–10^{-10}%, which are intermediate values between those of the dry and wet granite (Figs. 8C-D, Table 2).

3.1.4. *Wet quartzite*

We can observe that the strength profiles are very similar to those of the wet granite and dry quartzite, but the BDT depths are 1–2 km deeper, for each geotherm and strain rate value considered, despite being a

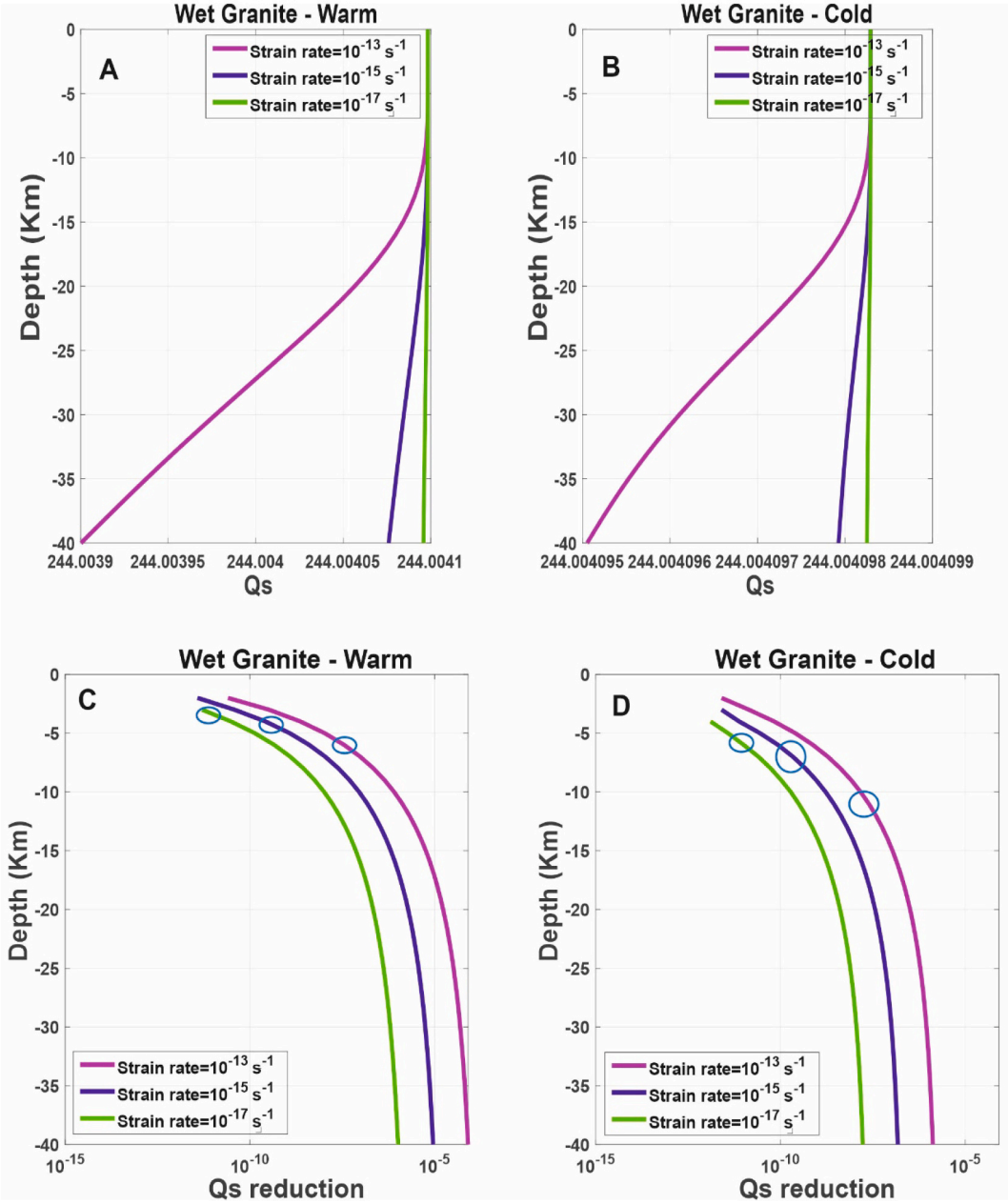

Fig. 6. Results of the numerical tests on wet granite rheology: **(A-B)** Q_s and **(C–D)** Q_s reduction (%) variation with depth, using three different values of strain rate and the **(A** and **C)** '*warm*' and **(B** and **D)** '*cold*' geotherm as input parameters. Light blue ellipses show the range of the BDT depth. See main text for further explanations. (For interpretation of the references to colour in this figure legend, the reader is referred to the web version of this article.)

hydrated rheology and supposed to be weaker than a granite rheology. As in case of the wet granite, the range of the BDT depth is reduced to 1 or 2 km, depending on the geotherm used, corresponding to a temperature range of 20–40 °C (Fig. 9A–B and Table 2). The mean η_s values at the BDT depths are within the same orders of magnitude than those of a wet granite (Fig. 9C–D), except for the case when the '*warm*' geotherm and a strain rate of 10^{-17} s^{-1} are used as input, for which the η_s is one order greater (Fig. 9C and Table 2). In contrast, the mean value in the *Qs* reduction have the same orders of magnitude observed in all the previous rheologies and starts at a depth range of 2–4 km and 3–6 km, depending on the input geotherm (Fig. 10C–D).

Below the BDT depth, we can observe that the maximum depth at which the strength decreases to <10 MPa is about 10 km and 30 km, when we use the '*warm*' and '*cold*' geotherm, respectively (Fig. 9a-b). Furthermore, the mean values of the η_s and Q_s reduction at the base of the crust show the same range observed for the wet granite, for each geotherm and strain rate used (Figs. 9C-D and 10C-D). Therefore, this rheology is stronger than that of the wet granite up to the BDT depth, while at greater depths shows a very similar behaviour.

3.2. *Mafic rocks*

3.2.1. *Dry diabase*

Looking at the strength envelopes computed for the '*warm*' geotherm, we can observe that this rheology is significantly stiffer than the sialic ones, reaching a maximum strength value of 1000 MPa at the BDT depth, which occurs below 5 km for each strain rate used (Fig. 11A and Table 2). In addition, for each strength envelope, the BDT depth spans a range of 2 km, while the corresponding temperature lies within 30–50 °C. Below the BDT depth, the strength strongly reduces, reaching

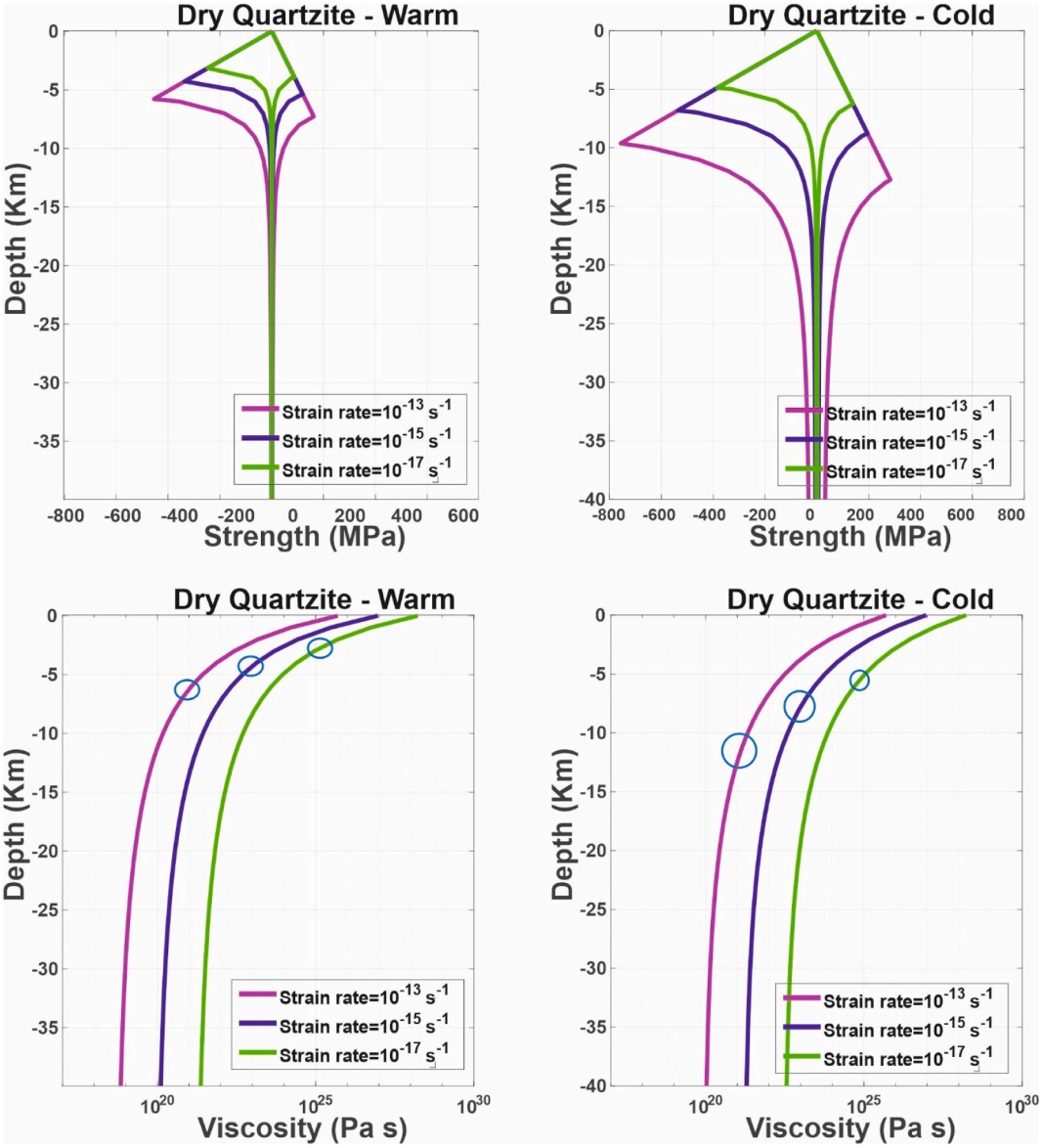

Fig. 7. Results of the numerical tests on dry quartzite rheology: **(A-B)** strength (MPa) and **(C–D)** viscosity (Pa s) variation with depth, using three different values of strain rate and the **(A** and **C)** '*warm*' and **(B** and **D)** '*cold*' geotherm as input parameters. Light blue ellipses show the range of the BDT depth. See main text for further explanations. (For interpretation of the references to colour in this figure legend, the reader is referred to the web version of this article.)

values <10 MPa at around 30 km for a strain rate of 10^{-13} s^{-1} (Fig. 11A). We can observe that when the '*cold*' geotherm is used as input, the difference between each strength envelope (and thus in the depth to the BDT), due to the different strain rate, is more remarkable. In particular, the maximum strength value is >1000 and > 2000 MPa for a strain rate of 10^{-17} s^{-1} and 10^{-13} s^{-1}, respectively. For the lowest value of strain rate, the BDT depth is between 15 and 18 km, while for the highest one, the rock shows only brittle deformation for extensional conditions and reaches the BDT at a depth of 26 km for compressional conditions (Fig. 11B). On the other hand, the temperatures range at which the BDT depth occurs is reduced to 30–40 °C (Table 2). Below the BDT depth, the strength at the base of the crust increases up to 1000 MPa for a strain rate of 10^{-13} s^{-1} and decreases, while remains relatively high, in the other cases (Fig. 11B).

The mean η_s values at the BDT depth span in the same ranges (10^{21}–10^{25} Pa s) for the '*warm*' and '*cold*' geotherm (in the last case considering only the strain rate values at which the BDT depth occurs), showing only a small increase in the orders of magnitude, compared to the previous cases (Fig. 11C and Table 2). We can further notice that the mean values of the Q_s reduction at the BDT depth show the same orders of magnitude of those of the rheologies already discussed (10^{-8}–10^{-12}%) for the '*warm*' geotherm and slightly increase for the '*cold*' geotherm (Figs. 12C-D and Table 2).

Below the BDT depths, the η_s profile shows a significant decrease up to the base of the crust when the '*warm*' geotherm is used (between 10^{19} and 10^{22} Pa s), while the decrease is significantly smaller (between 10^{21} and 10^{24} Pa s) for the '*cold*' geotherm scenario, demonstrating the stiffness of this rheology (Figs. 11C-D). In a similar way, the Q_s reduction increases up to 10^{-9}–10^{-6}% when the '*warm*' geotherm is the input, and only slightly, up to 10^{-11}–10^{-8}% in the other case (Fig. 12C-D).

When using the '*warm*' geotherm as input, the Q_s starts to reduce at a depth between 4 and 9 km, while for the other geotherm the Q_s reduction starts at greater depths, at about 16 km for the lowest value of strain rate. We can also notice that the gradient of Q_s reduction at a depth > 20 km becomes almost negligible, in particular when the '*cold*' geotherm and strain rate of 10^{-17} s^{-1} are used as input (Fig. 12D).

Dry OPX: We can observe that the strength is remarkably higher than that of the diabase, with a maximum strength value of about 1500 MPa

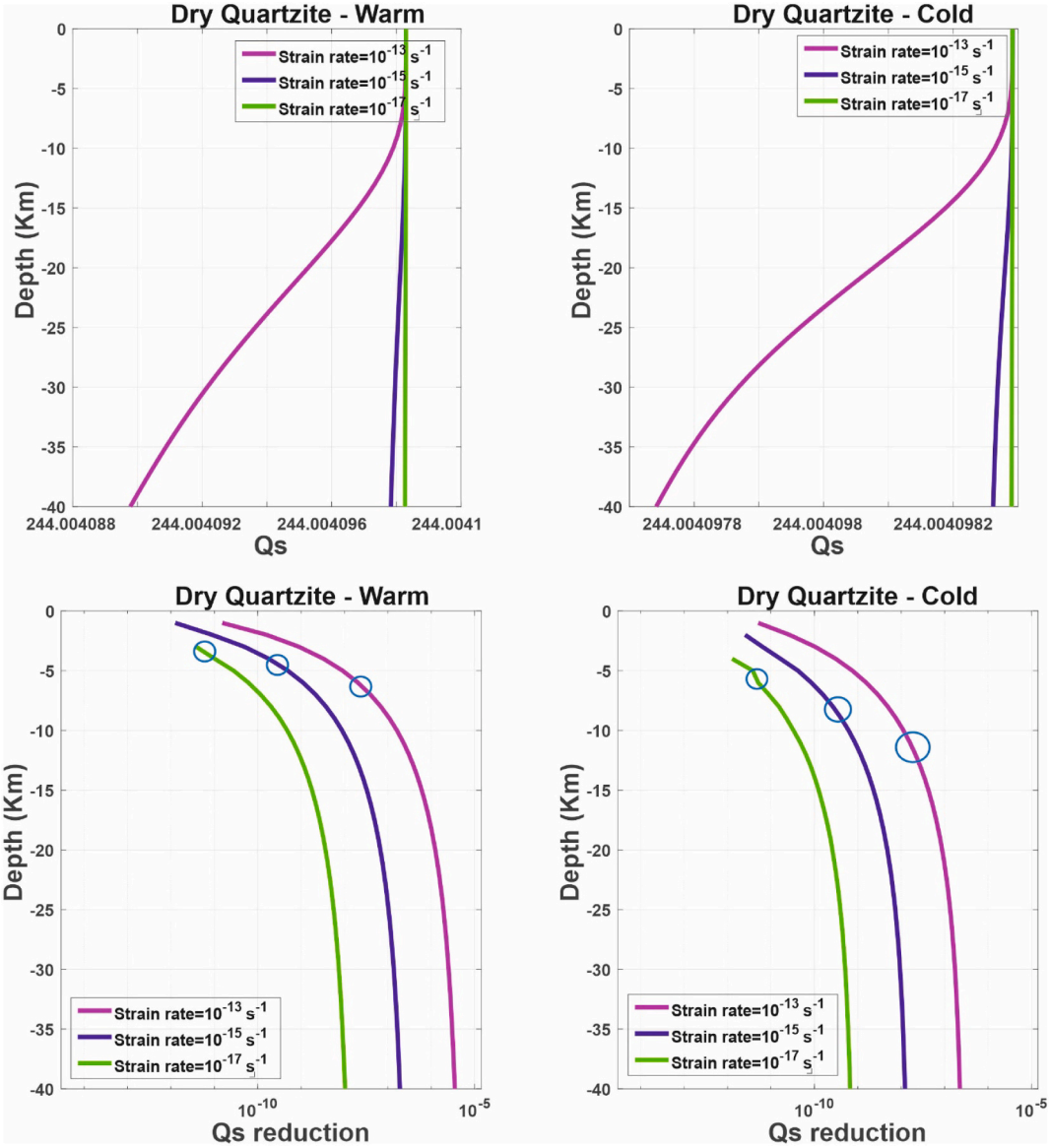

Fig. 8. Results of the numerical tests on dry quartzite rheology: **(A-B)** Q_s and **(C–D)** Q_s reduction (%) variation with depth, using three different values of strain rate and the **(A** and **C)** '*warm*' and **(B** and **D)** '*cold*' geotherm as input parameters. Light blue ellipses show the range of the BDT depth. See main text for further explanations. (For interpretation of the references to colour in this figure legend, the reader is referred to the web version of this article.)

at the BDT depth, occurring at 15 km for the '*warm*' geotherm and a strain rate of 10^{-13} s^{-1} (Figs. 13A). Therefore, the temperatures intercepting the BDT depth are higher than those of the dry diabase, but the range of variation for each strength envelope is smaller (about 20–35 °C), since it corresponds to a BDT depth range of only 1–2 km (Table 2). Below the BDT depth, the strength rapidly decreases reaching values <10 MPa at about 35 km for a strain rate of 10^{-13} s^{-1} (Fig. 13A). The stiffness of the rheology is even more evident looking at the '*cold*' strength envelopes, showing that the depth of the BDT is reached only for the smallest value of strain rate at depth > 20 km, while for greater values of strain rate, the rock deforms only in brittle conditions (Fig. 13B). Therefore, the strength at the base of the crust increases up to almost 4000 MPa in compressional conditions, for a strain rate of 10^{-13} s^{-1}.

In addition, while the mean η_s values at the BDT depth and base of the crust for the '*warm*' geotherm are of the same order of magnitude than those of the dry diabase, those at the base of the crust for the '*cold*' geotherm are of one order of magnitude higher (10^{22}–10^{25} Pa s, respectively), Figs. 13C-D. Similarly, mean values of the Q_s reduction at the BDT depths have the same orders of magnitude than those obtained from the dry diabase, while the values at the base of the crust are similar to those of the dry diabase, only in case the '*warm*' geotherm is used (Fig. 14C). In in the other case, the values of the Q_s reduction are one order of magnitude smaller (between 10^{-9}–10^{-12}%, Fig. 14D). In addition, reduction in the Q_s starts to occur at a depth between 5 and 10 km when the '*warm*' geotherm is the input, while at greater depths, between 11 and 25 km, for the other cases. Below 25 km, the Q_s reduction gradient becomes very small in all cases (Fig. 14C-D).

3.2.2. *Dry CPX*

The strength envelopes displayed in Figs. 15A-B show that the CPX is the stiffest rheology among those analysed. Using the '*warm*' geotherm as input, the maximum strength is higher than that of the dry OPX and the BDT occurs at a variable depth, between a minimum of 12–15 km and a maximum of 16–23 km, for the lowest and highest strain rate, respectively. The depth of the BDT range is also significantly increased, compared to the previous rheologies, as well as the corresponding temperature range, which is between 60 and 90 °C (Table 2). Below the

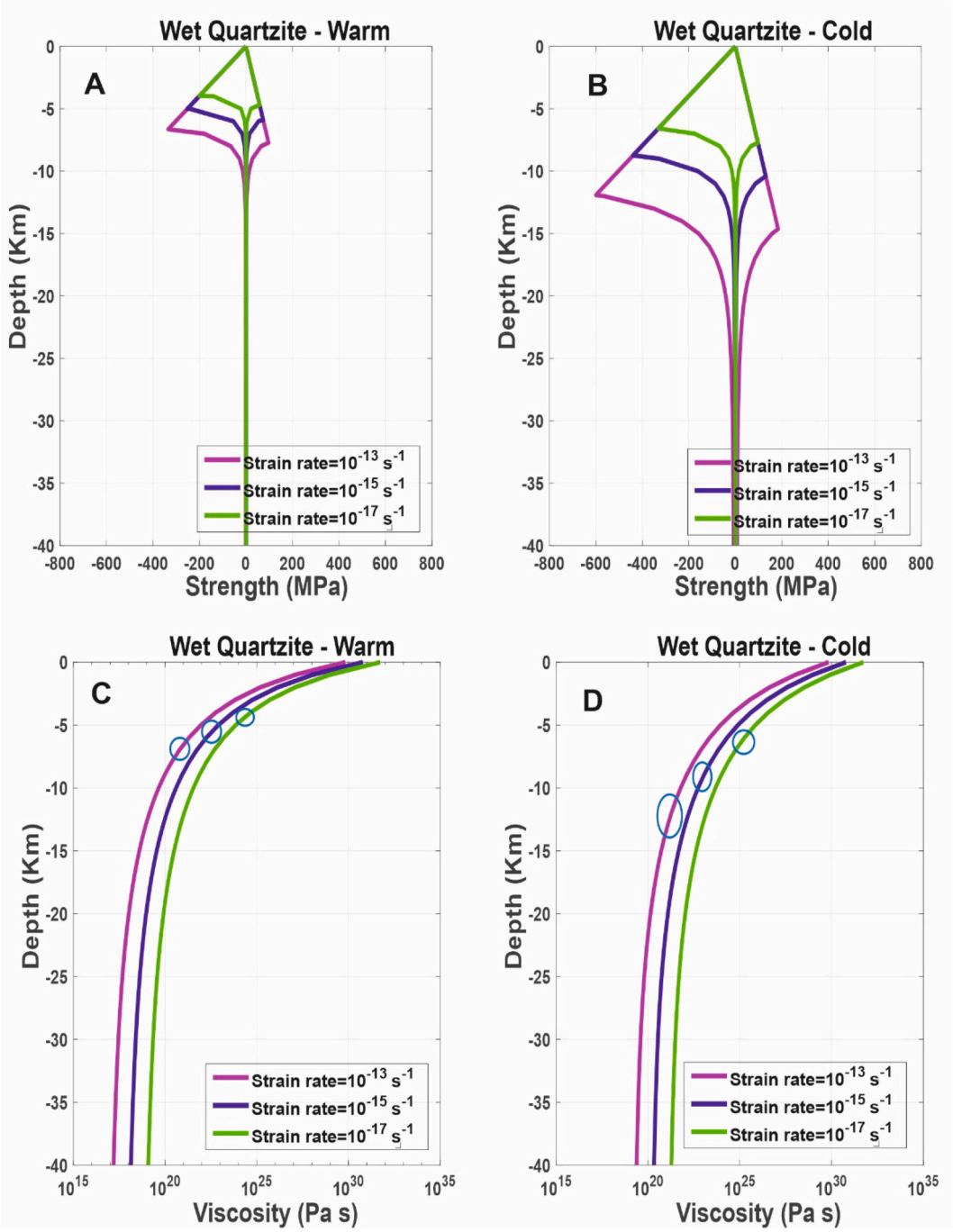

Fig. 9. Results of the numerical tests on wet quartzite rheology: **(A-B)** strength (MPa) and **(C–D)** viscosity (Pa s) variation with depth, using three different values of strain rate and the **(A** and **C)** '*warm*' and **(B** and **D)** '*cold*' geotherm as input parameters. Light blue ellipses show the range of the BDT depth. See main text for further explanations. (For interpretation of the references to colour in this figure legend, the reader is referred to the web version of this article.)

BDT, the strength remains relatively high till the base of the crust for a strain rate of 10^{-13} s^{-1} (Fig. 15A). When the '*cold*' geotherm is used as input, the BDT is never reached for extensional stress conditions, while, for compressional conditions, it is only reached for strain rate values of 10^{-15} and 10^{-17} s^{-1}. The mean η_s values at the BDT depth are of the same order of magnitude of the other two mafic rheologies, while at the base of the crust they are higher of one order of magnitude only when the '*warm*' geotherm is the input (Figs. 15C-D).

The mean values of the Q_s reduction at the BDT depth are of the same orders of magnitude than those of the previous rheologies and higher by one-two orders of magnitude at the base of the crust for the '*warm*' geotherm. We can further notice that the Q_s reduction starts to increase with a very small gradient at higher depths than those of the dry OPX, demonstrating the higher stiffness of this rheology (Figs. 16C-D). In particular, when the '*cold*' geotherm is used as input, reduction in the Q_s starts only at 34 km, for a strain rate of 10^{-17} s^{-1} (Fig. 16D).

3.3. *Dependency of the shear quality factor (Q_s) on temperature, strain rate, and rheology of the crustal rocks*

After describing, in the above sections, the differences in the Q_s values, between the rock's rheologies at the thermal and strain rate condition assumed, we intend to investigate the general trend of the seismic attenuation with respect to the same parameters. To this

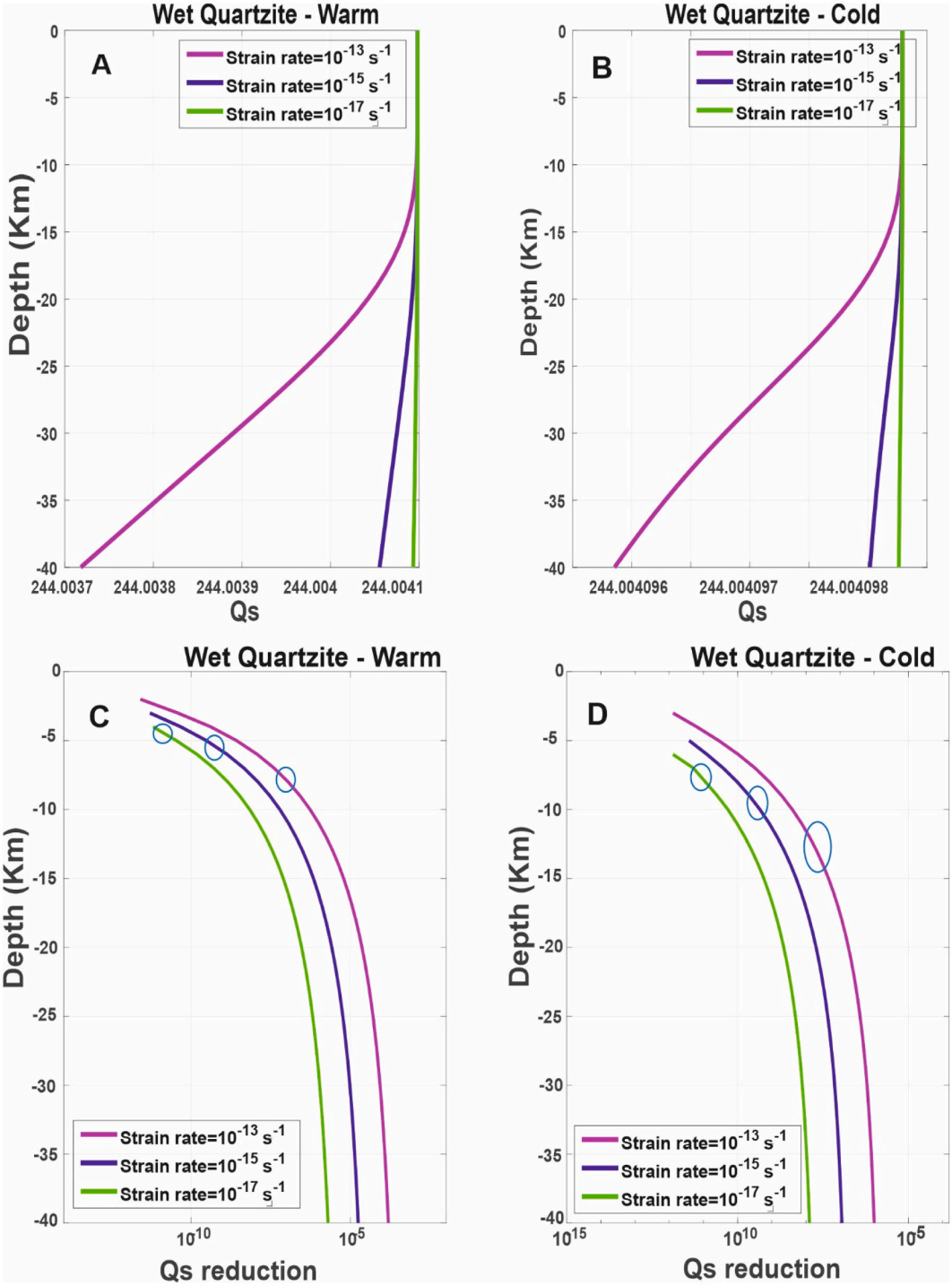

Fig. 10. Results of the numerical tests on wet quartzite rheology: **(A-B)** Q_s and **(C–D)** Q_s reduction (%) variation with depth, using three different values of strain rate and the **(A** and **C)** '*warm*' and **(B** and **D)** '*cold*' geotherm as input parameters. Light blue ellipses show the range of the BDT depth. See main text for further explanations. (For interpretation of the references to colour in this figure legend, the reader is referred to the web version of this article.)

purpose, we display the Q_s variations with respect to temperature, computed for all the rheologies, at the different strain rate conditions, (Figs. 17A). We can observe that the Q_s variations occurring at low temperatures (< 400 °C), generally corresponding to the brittle rock's deformation domain, are confined in a small range. The differences between the rock's rheologies can be hardly detected, since the values tend to overlap. On the other hand, at temperatures over 400 °C, where ductile deformation occurs, the Q_s values decrease. This is particularly evident for the hydrous rheologies at maximum strain rate assumed (10^{-13} s^{-1}).

In order to improve our understanding on the dependency of the Q_s on the different parameters, we display the Q_s variations with respect to temperature, for each strain rate value, and fit the curves with a polynomial function (Figs. 17B-D). We establish as a fit quality criterium, that the determination coefficient (R^2) has to exceed a threshold of 0.95. We can first observe that a significant decrease of the Q_s at temperature above 400 °C occurs for the hydrous rheology for each value of strain rate considered. On the other hand, the range of the Q_s variations for the

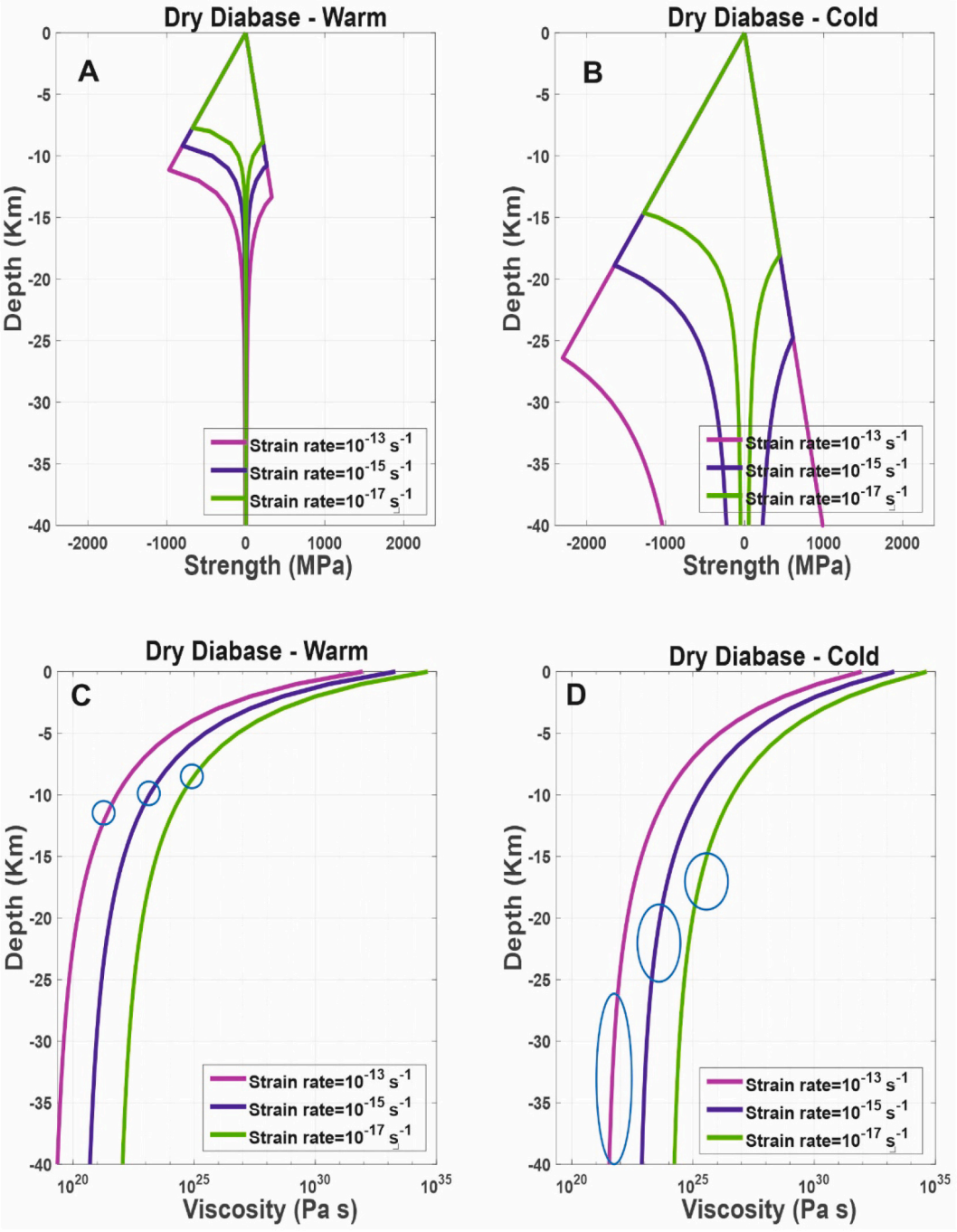

Fig. 11. Results of the numerical tests on dry diabase rheology: **(A-B)** strength (MPa) and **(C–D)** viscosity (Pa s) variation with depth, using three different values of strain rate and the **(A** and **C)** '*warm*' and **(B** and **D)** '*cold*' geotherm as input parameters. Light blue ellipses show the range of the BDT depth. See main text for further explanations. (For interpretation of the references to colour in this figure legend, the reader is referred to the web version of this article.)

anhydrous rheologies becomes narrower by decreasing the strain rate value (Fig. 17B-D). Despite these differences, as displayed in Table 3, the best fit of all the curves is obtained using a polynomial function of 3rd order. This means that, although the Q_s variations with temperature depend on the rock's rheology (Figs. 17B-D), the trend is defined by the same type of polynomial function. This is not surprising, considering that we assumed that the rocks deform in ductile conditions according to the same type of flow law.

4. Discussion

The rheological behaviour and deformation mechanisms of rocks (both single crystals and polycrystalline aggregates) have been extensively investigated (e.g., Goetze and Evans, 1979; Carter and Tsenn, 1987; Wilks and Carter, 1990; Fernandez and Ranalli, 1997; Afonso and Ranalli, 2004; Burgmann and Dresen, 2008). The results of these studies have established how hydrated rocks are characterized by a generally weaker rheology than the corresponding anhydrous ones and how sialic rocks are less stiff than mafic rocks (e.g., Fernandez and Ranalli, 1997; Burov, 2011). Furthermore, several studies have explored systematically the effects of composition, temperature, deformation mechanism, and tectonic regime on strength variation and, in particular, on the depth to the BDT (e.g., Burov, 2011).

In this study, we have investigated the relation between variations in

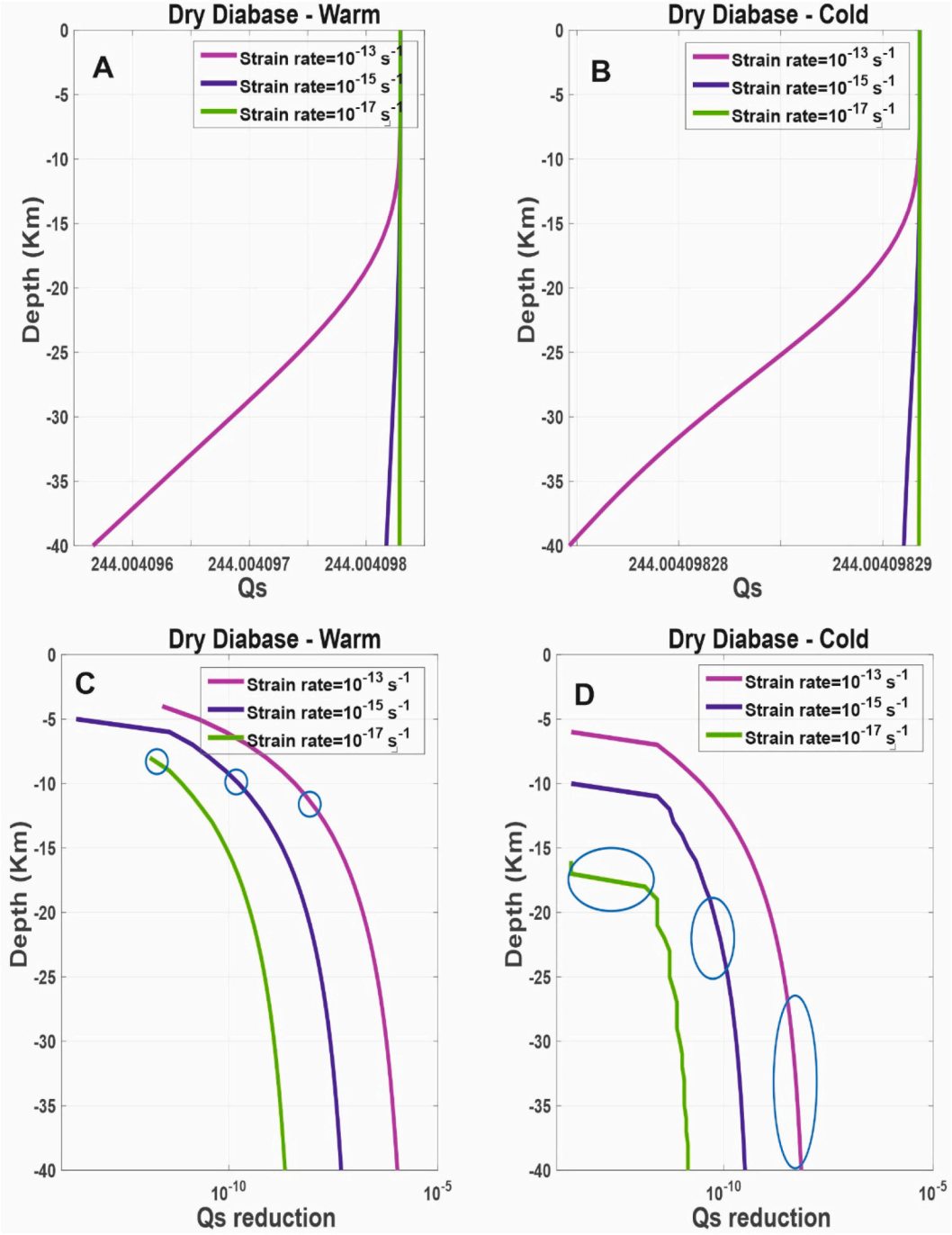

Fig. 12. Results of the numerical tests on dry diabase rheology: **(A-B)** Q_s and **(C–D)** Q_s reduction (%) variation with depth, using three different values of strain rate and the **(A** and **C)** *'warm'* and **(B** and **D)** '*cold*' geotherm as input parameters. Light blue ellipses show the range of the BDT depth. See main text for further explanations. (For interpretation of the references to colour in this figure legend, the reader is referred to the web version of this article.)

the rock's strength and seismic attenuation. To this purpose, we have used the Burgers and Gassmann model to compute the Q_s from the η_s, the latter obtained by computing the ductile strength for different rock's compositions, strain rate values, and thermal conditions. In addition, we have used the same input parameters to compute the YSEs, in order to quantify the sensitivity of the Q_s on the depth to the BDT and resolved ductile strength.

We have observed that among the tested rheologies of the sialic rocks, the dry granite is the stiffest, being characterized by the greatest BDT depth (up to a maximum of 19 km, Fig. 3A and Table 2) and highest values of yield strength at the BDT depth (up to a maximum of 1000 MPa, Fig. 3A). The other sialic rheologies show similar strength profiles and BDT depths, due to their similar response, expressed in term of strength variations, to the input temperatures and strain rate. In addition, the BDT depths, for each strength envelope, span a relatively wide range (up to 5 km) only for the dry granite, while for the other rheologies the depth range is reduced to 1–2 km (Table 2). We can further notice that the ranges of the BDT depth tend to increase for the '*cold*' geotherm and highest strain rate values (Fig. 3B), while the T_{BDT} is more sensitive to the input strain rate and varies within a relatively narrow range, between about 20 and 60 °C (Table 2).

Despite the differences in the strength envelopes, related to the

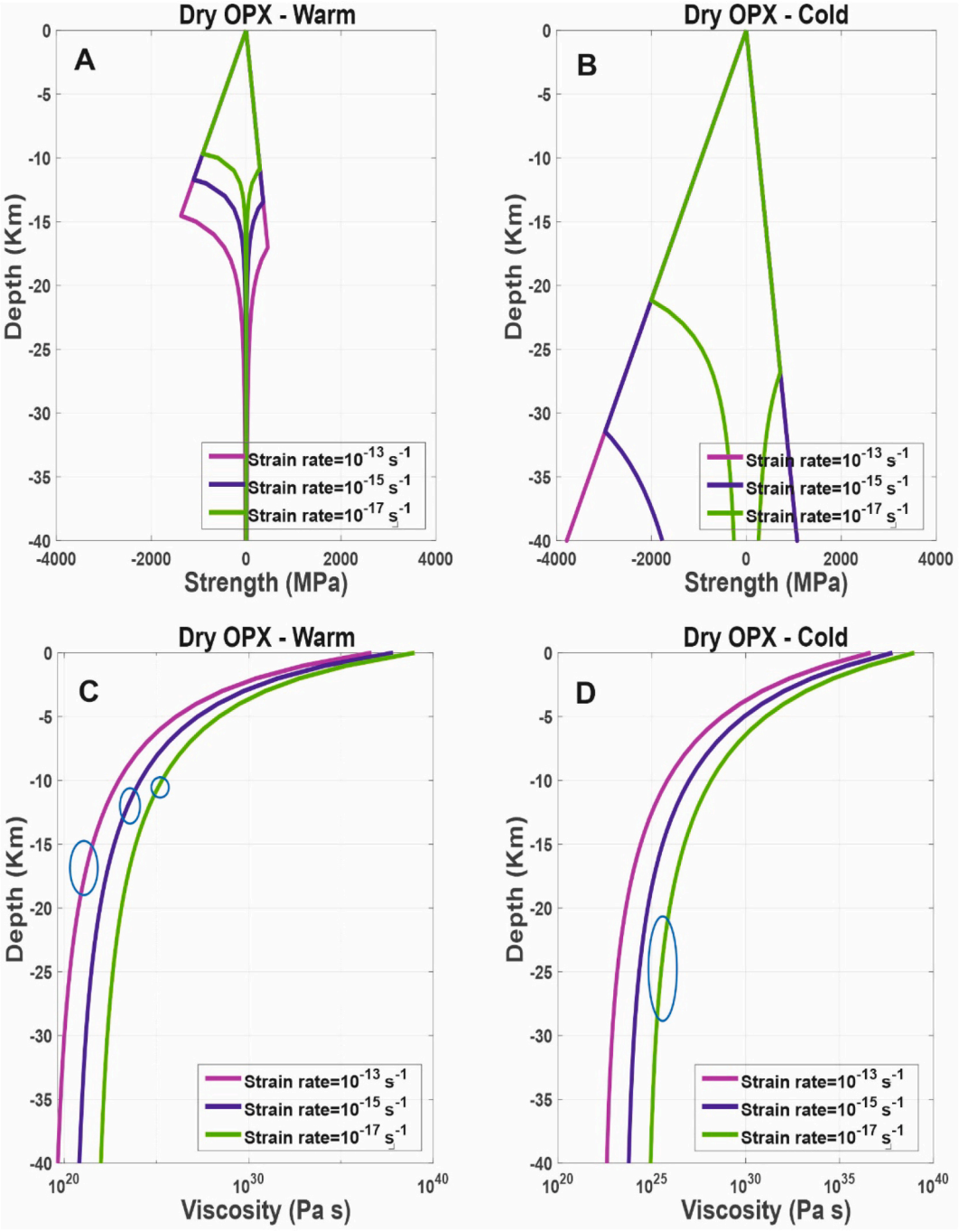

Fig. 13. Results of the numerical tests on dry OPX rheology: **(A-B)** strength (MPa) and **(C–D)** viscosity (Pa s) variation with depth, using three different values of strain rate and the **(A** and **C)** '*warm*' and **(B** and **D)** '*cold*' geotherm as input parameters. Light blue ellipses show the range of the BDT depth. See main text for further explanations. (For interpretation of the references to colour in this figure legend, the reader is referred to the web version of this article.)

change of the input parameters, we found that the mean values of the η_s at the depth of the BDT remain almost constant for the same strain rate value (Table 2). An increase by two orders of magnitude in strain rate results in approximately the same amount of decrease in the mean η_s at the BDT depth. At the same depth, the mean value in the reduction of the Q_s shows a direct proportionality with the imposed strain rate values, while it seems to be less affected by changes in the other input parameters. Therefore, reduction in the Q_s at the BDT depth is characterized by a specific order of magnitude for each strain rate value (10^{-12}, 10^{-10}, and 10^{-8}% for strain rate equal to 10^{-17}, 10^{-15}, and 10^{-13} s^{-1}, respectively).

As expected, below the BDT depth, the yield strength reduces to negligible values (< 10 MPa), faster for hydrated rheology and when the '*warm*' geotherm and lowest strain rate value are used (Figs. 5A and 9A). In a similar fashion, also the η_s values and reduction in the Q_s, at the base of the crust, vary by some orders of magnitudes, depending on the input parameters. In addition, η_s minima (10^{17} and 10^{19} Pa s) and Q_s reduction maxima (10^{-6}–10^{-4}%) are observed when the '*warm*' geotherm and strain rate value of 10^{-13} $s^{-1}$are the input. Among the sialic rheologies, the wet granite appears to be the weakest, being characterized by a η_s and Q_s reduction, at the base of the crust, similar to those of the wet quartzite, but showing a lower amount of yield strength (Figs. 5A-B).

In contrast, mafic rheologies deform prevalently in brittle conditions and their strength envelopes are characterized by maxima of the order of

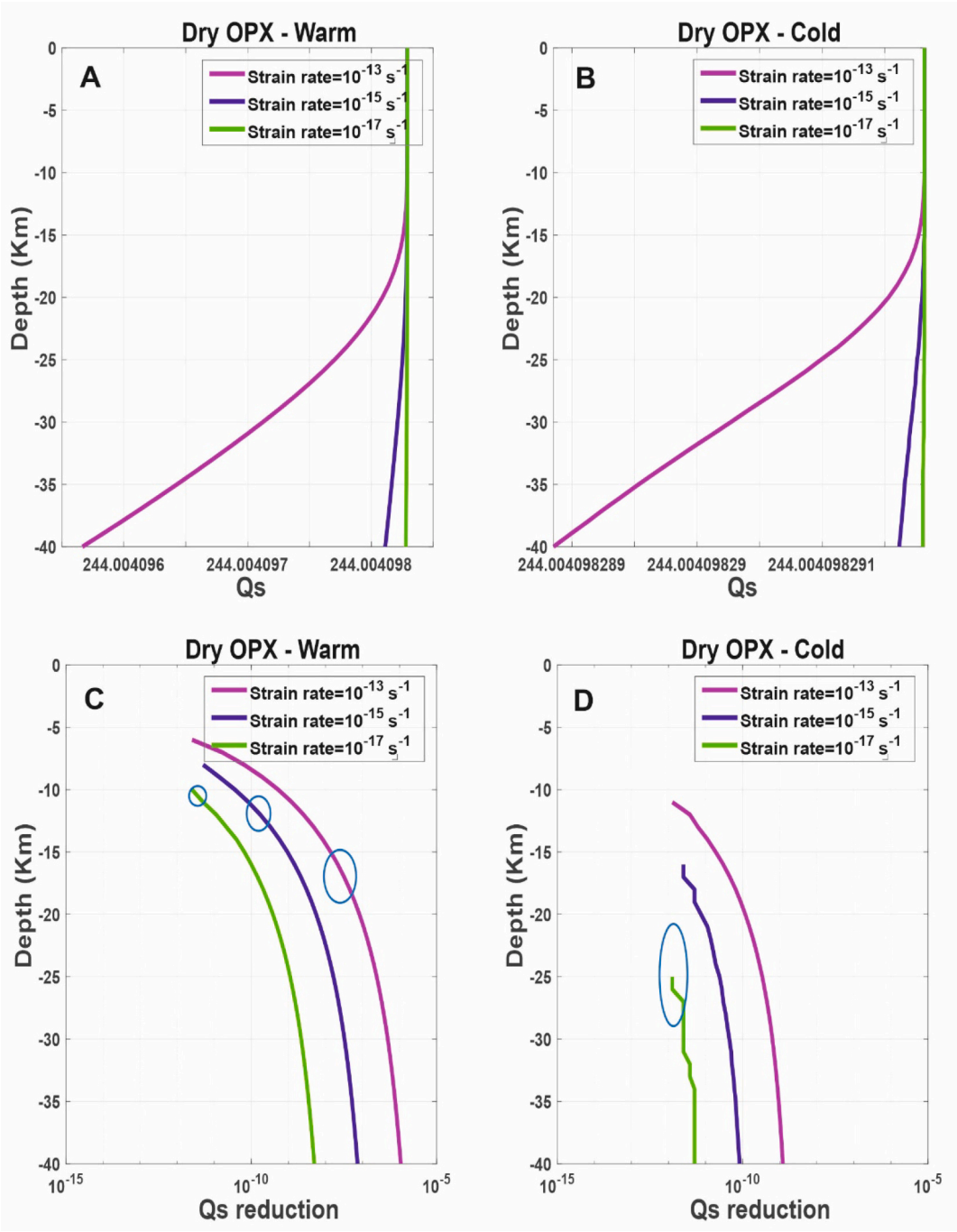

Fig. 14. Results of the numerical tests on dry OPX rheology: **(A-B)** Q_s and **(C–D)** Q_s reduction (%) variation with depth, using three different values of strain rate and the **(A** and **C)** '*warm*' and **(B** and **D)** '*cold*' geotherm as input parameters. Light blue ellipses show the range of the BDT depth. See main text for further explanations. (For interpretation of the references to colour in this figure legend, the reader is referred to the web version of this article.)

1000 MPa, associated to deeper BDT depths (usually >10 km). In particular, when we consider the '*cold*' geotherm, a strain rate value of 10^{-15} s^{-1} or greater, and assume extensional stress conditions, the selected mafic rocks deform only in brittle conditions (Figs. 11B, 13B, and 15B). We can further observe that the depths to the BDT, when occur, and the intercepting temperatures span a range greater than those obtained for sialic rocks (up to 6 km and 80–90 °C, respectively, Table 2). In the same way, the η_s values at the BDT depth are approximately one order of magnitude greater than those associated to the sialic rheologies (Table 2). As in the previous case, they proportionally increase with decreasing strain rate (10^{21}, 10^{23}, and 10^{25} Pa s, for a strain rate of 10^{-13}, 10^{-15}, and 10^{-17} s^{-1}). The mean reduction in the Q_s at the BDT depth for each value of strain rate are similar to those obtained for the sialic rocks, when the '*warm*' geotherm is used, and slightly lower in case of the '*cold*' geotherm, showcasing a weak dependency of this parameter to the input thermal conditions and rheology. Below the BDT depth, the η_s reduces at the base of the crust to values of 10^{19}–10^{21} Pa s, while the reduction in the Q_s increases up to 10^{-7}–10^{-6}%, for the '*warm*' geotherm and strain rate value of 10^{-13} s^{-1}. Therefore, we could demonstrate, in agreement with previous studies (e.g., Farina et al., 2019), that the attenuation significantly increases (i.e., the Q_s significantly decreases) when the rock is in a fully ductile regime of deformation. Furthermore, variations in the Q_s, at the BDT depth are less affected by the input rheology and geotherm than variations in the η_s.

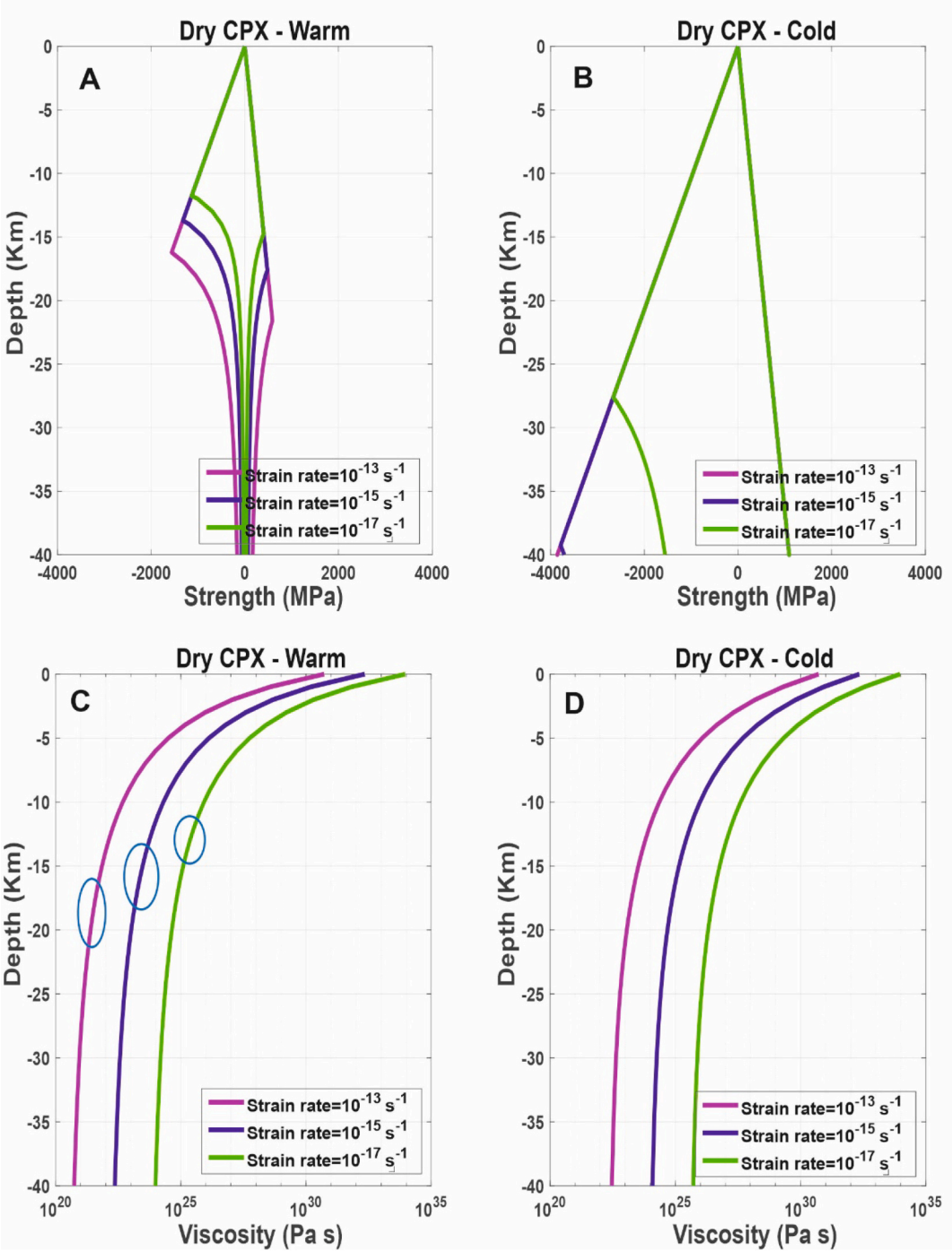

Fig. 15. Results of the numerical tests on dry CPX rheology: **(A-B)** strength (MPa) and **(C–D)** viscosity (Pa s) variation with depth, using three different values of strain rate and the **(A** and **C)** '*warm*' and **(B** and **D)** '*cold*' geotherm as input parameters. Light blue ellipses show the range of the BDT depth. See main text for further explanations. (For interpretation of the references to colour in this figure legend, the reader is referred to the web version of this article.)

The implication is that, by knowing the average strain rate of an area, variations in the Q_s can provide a useful attribute to identify the domain within the crust, where the deformation transitions from a brittle dominated to a more ductile deformation mode. In addition, this extrapolation is subjected to less uncertainties than other proxies in terms of variations of *P-T* conditions and flow law parameters.

Furthermore, we can generally notice that the Q_s starts to decrease with respect to its surface value, when the rock deforms in brittle conditions (above the depth of the BDT), with high gradients, until the depth of the transition to the ductile regime. In case the crust deforms only in brittle conditions, the Q_s starts to reduce at great depths (between 6 and 34 km, depending on the rheology and strain rate value), usually with a high gradient only in the first kilometers. At the base of the crust, the Q_s shows very small reductions (10^{-9}–10^{-8}%), also for the highest strain rate value (Fig. 16D), while η_s remains relatively high (10^{20}–10^{22} Pa s).

On the other hand, we should consider that the computed YSEs, and thus the depth at which the BDT occurs, are affected by uncertainties on rock's mechanics data and knowledge of our real deformation mechanisms occurring at depth (e.g., Burov, 2011). Indeed, lab experiments, used to compute our YSEs, are conducted on simple monophase minerals or selected 'representative' rocks and refer to simplified confining

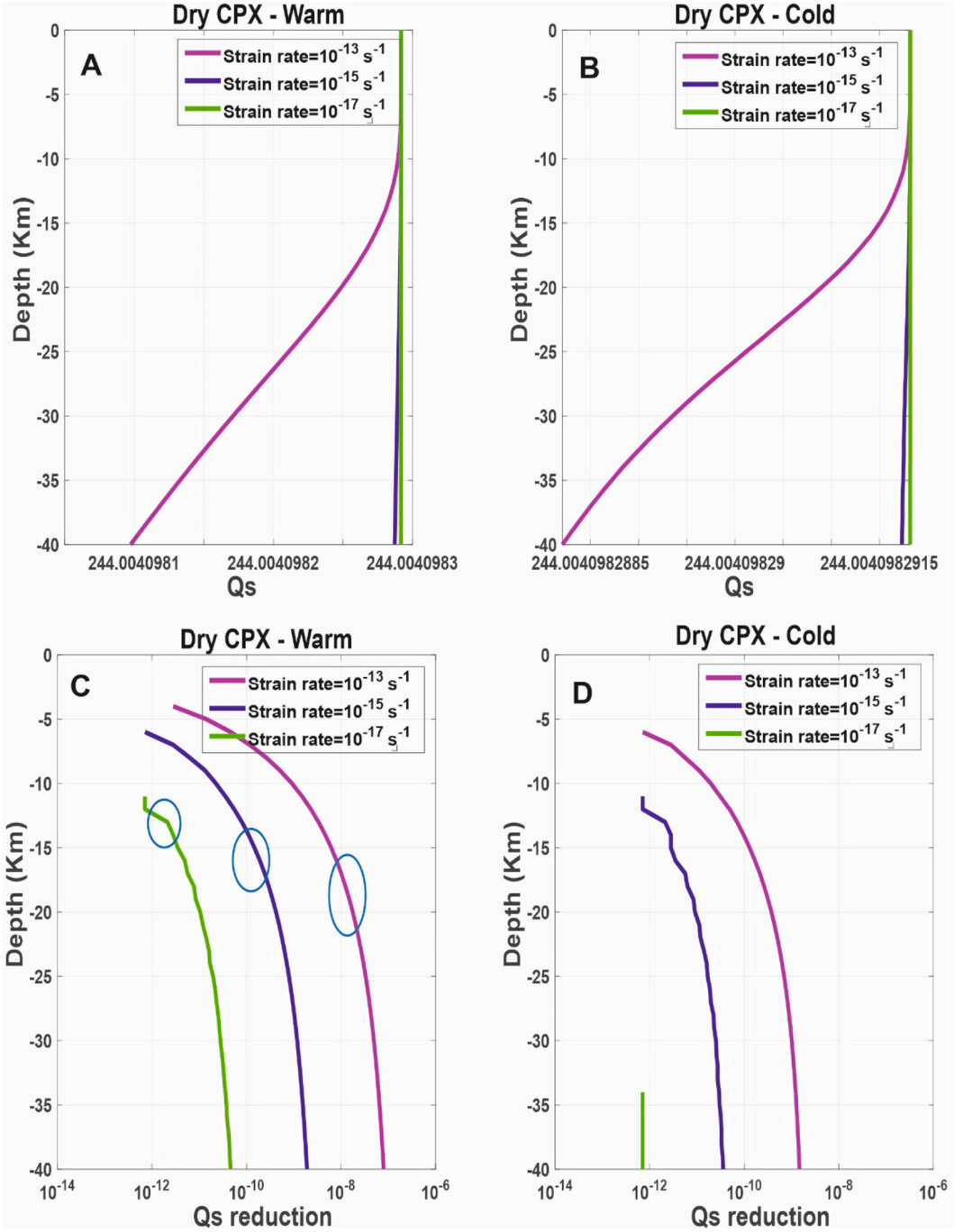

Fig. 16. Results of the numerical tests on dry granite rheology: **(A-B)** Q_s and **(C–D)** Q_s reduction (%) variation with depth, using three different values of strain rate and the **(A** and **C)** '*warm*' and **(B** and **D)** '*cold*' geotherm as input parameters. Light blue ellipses show the range of the BDT depth. See main text for further explanations. (For interpretation of the references to colour in this figure legend, the reader is referred to the web version of this article.)

conditions, such as uniaxial deformation. In contrast, real rocks display a heterogeneous composition and are subjected to deformation along several planes (true triaxial deformation). In addition, creep parameters are obtained from lab experiments conducted at *T-P* and strain rate conditions, which are not representative of natural tectonic conditions at which crustal rocks deform (e.g., Burov, 2011). Despite these aspects, the results from this study have revealed that the orders of magnitude of the Q_s reduction, referring to variable ranges of the BDT depth, are sensitive only to the imposed strain rate. Indeed, although they are very small, they remain constant, for all types of rheology and thermal conditions. This again significantly reduces the effect of uncertainties in the derivation of the depth of the BDT on the obtained results.

Other important results of this study are the empirical relationships describing the Q_s variations with temperature that we derived for the different rock's rheology and strain rate values. We demonstrated that the Q_s variation as function of temperature can be quantitative described via a 3rd order polynomial function, determined by the rock's rheology and, only to a lesser extent, by the imposed strain rate conditions. This allows us to extend the validity of our results over the range of values of the rock's parameters assumed. Concerning the applicability of the results to natural cases, we should consider that the crust of cratonic areas are usually characterized by a low amount of radiogenic heat (and thus of temperature gradient), and usually by a dry and therefore stiff rheology (e.g., Mareschal and Jaupart, 2004; Tesauro et al., 2015),

Table 2
Range of the brittle-ductile transition (BDT) depth and intercepting temperatures (T_{BDT}), mean values of the shear viscosity (η_s) and shear wave attenuation (Q_s) at the BDT depth for the seven rheologies chosen at thermal conditions defined by the '*warm*' and '*cold*' geotherm, respectively, and three input strain rate values. See main text for further explanations.

Lithology	Strain rate	Warm Geotherm				Cold Geotherm			
		Range of the BDT depth (Compressional-Extensional regime) km	Range of the T_{BDT} °C	Mean η_s at the BDT depth Pa s	Mean Q_s reduction at the BDT depth %	Range of the BDT depth (Compressional- Extensional regime) km	Range of the T_{BDT} °C	Mean η_s at the BDT depth Pa s	Mean Q_s reduction at the BDT depth %
Dry Granite	E^{-13} s^{-1}	8–10	330–388	$1.05E^{21}$	$2.70E^{-08}$	14–19	291–339	$2.23E^{+21}$	$1.20E^{-08}$
	E^{-15} s^{-1}	6–7	264–298	$1.17E^{+23}$	$2.38E^{-10}$	10–14	237–291	$1.76E^{+23}$	$1.68E^{-10}$
	E^{-17} s^{-1}	5–6	227–264	$7.00E^{+24}$	$5.06E^{-12}$	8–10	202–237	$1.34E^{+25}$	$2.53E^{-12}$
Wet Granite	E^{-13} s^{-1}	6–7	264–298	$4.60E^{+20}$	$6.64E^{-08}$	10–12	237–266	$1.08E^{+21}$	$2.58E^{-08}$
	E^{-15} s^{-1}	4–5	188–227	$5.64E^{+22}$	$7.29E^{-10}$	7–9	183–220	$6.27E^{+22}$	$5.41E^{-10}$
	E^{-17} s^{-1}	3–4	145–188	$3.30E^{+24}$	$1.78E^{-11}$	6–5	140–163	$5.01E^{+24}$	$6.98E^{-12}$
Dry Quartzite	E^{-13} s^{-1}	6–7	264–299	$8.97E^{+20}$	$3.00E^{-08}$	10–13	237–279	$1.42E^{+21}$	$1.90E^{-08}$
	E^{-15} s^{-1}	4–5	188–227	$9.21E^{+22}$	$3.36E^{-10}$	7–9	183–220	$1.01E^{+23}$	$2.80E^{-10}$
	E^{-17} s^{-1}	3–4	145–188	$5.81E^{+24}$	$6.97E^{-12}$	5–6	140–163	$8.05E^{+24}$	$4.44E^{-12}$
Wet Quartzite	E^{-13} s^{-1}	7–8	298–330	$1.32E^{+21}$	$7.56E^{-08}$	11–13	266–302	$1.08E^{+21}$	$2.77E^{-08}$
	E^{-15} s^{-1}	5–6	227–264	$4.92E^{+22}$	$8.19E^{-10}$	8–10	220–252	$6.38E^{+22}$	$5.03E^{-10}$
	E^{-17} s^{-1}	5–4	188–227	$2.67E^{+24}$	$2.02E^{-12}$	6–7	183–202	$4.01E^{+24}$	$8.26E^{-12}$
Dry Diabase	E^{-13} s^{-1}	11–13	414–461	$2.22E^{+21}$	$1.30E^{-08}$	26 – >40	–	–	–
	E^{-15} s^{-1}	9–11	360–414	$1.70E^{+23}$	$1.92E^{-10}$	19–25	339–375	$3.29E^{+23}$	$8.26E^{-11}$
	E^{-17} s^{-1}	7–8	330–360	$1.08E^{+25}$	$2.54E^{-12}$	15–18	302–331	$2.42E^{+25}$	$3.33E^{-13}$
Dry OPX	E^{-13} s^{-1}	15–17	502–537	$2.44E^{+21}$	$2.24E^{-08}$	–	–	–	–
	E^{-15} s^{-1}	12–13	438–461	$2.14E^{+23}$	$2.52E^{-10}$	–	–	–	–
	E^{-17} s^{-1}	10–11	388–414	$1.42E^{+25}$	$3.77E^{-12}$	21–27	353–383	$4.09E^{+25}$	$7.22E^{-13}$
Dry CPX	E^{-13} s^{-1}	16–22	520–607	$3.24E^{+21}$	$1.53E^{-08}$	–	–	–	–
	E^{-15} s^{-1}	14–18	482–553	$2.50E^{+23}$	$1.98E^{-10}$	–	–	–	–
	E^{-17} s^{-1}	12–15	438–502	$2.14E^{+25}$	$2.29E^{-12}$	–	–	–	–

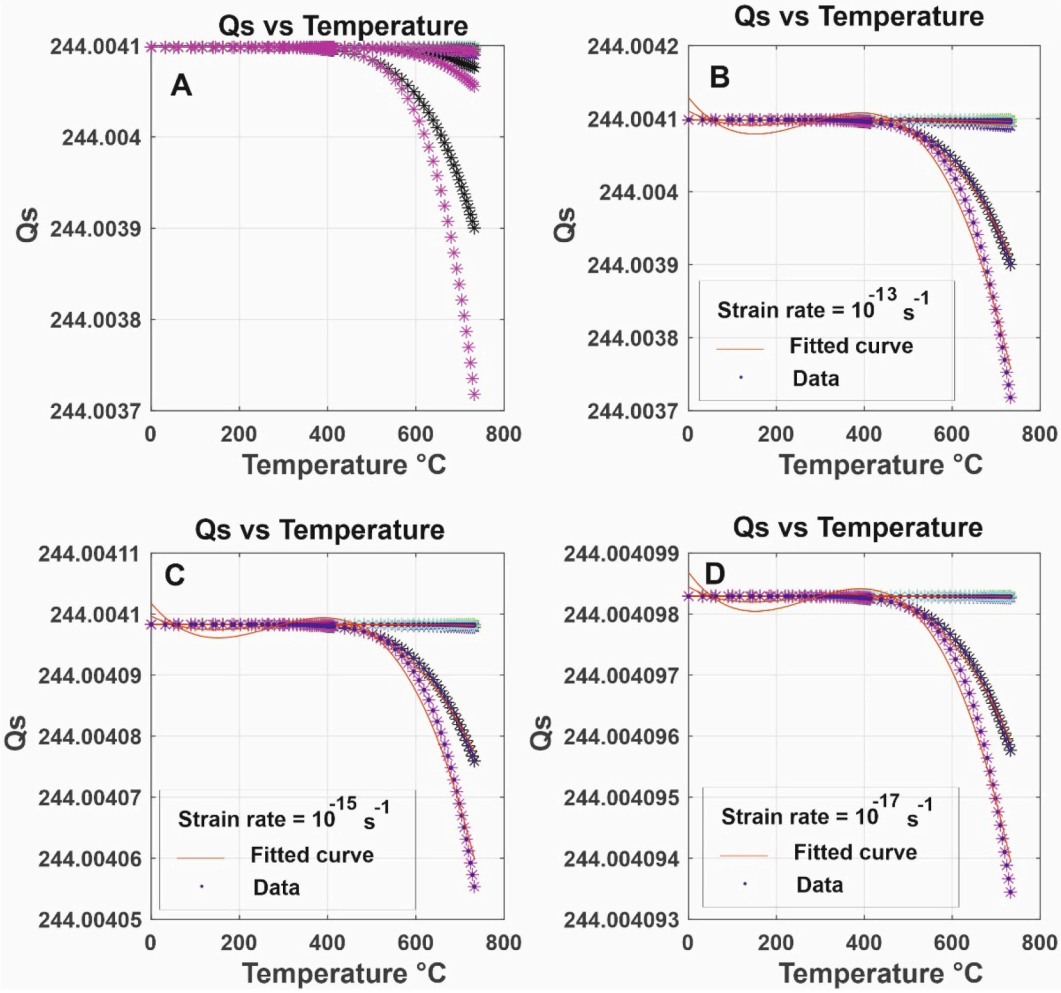

Fig. 17. Q_s variations with respect to temperature, for **(A)** all the tested rheologies, thermal and strain rate conditions assumed, and fitted by a polynomial function of 3rd order, for strain rate equal to **(B)** 10^{-13}, **(C)** 10^{-15}, **(D)** 10^{-17} s^{-1}, respectively. Colored asterisks show the data corresponding to the following rheologies: *Dry granite* (in red), *Dry quartzite* (in blue), *Dry Diabase* (in yellow), *Dry CPX* (in green), *Dry OPX* (in light blue), *Wet Granite* (in black), *Wet Quartzite* (in violet).

which would reduce their deformation in response to the plate boundary forces (e.g., Tesauro et al., 2015). For these reasons, the shallow parts of cratons are expected to deform prevalently in brittle conditions (e.g., Tesauro et al., 2015). This occurs despite the fact these areas are usually affected by low strain rate (10^{-17} s^{-1} or lower, Kreemer et al., 2014) and compressional stress conditions (e.g., Zoback and Mooney, 2003), which would both favour ductile deformation. In addition, considering that low strain rate values prevent significant reduction in the Q_s (i.e. increase of attenuation), we can conclude that the general thermophysical conditions of cratonic areas would make hard the detection of the BDT depth through the Q_s estimation.

In contrast, tectonically active areas, being affected by higher strain rate, in the order of 10^{-13} s^{-1} (Kreemer et al., 2014), and hotter thermal conditions, with respect to stable cratons (e.g., Mareschal and Jaupart, 2004; Mareschal and Jaupart, 2013), are domains where the BDT depth can be effectively detected through mapped reductions in the Q_s. Since the depth to the BDT provides a conservative lower bound to the seismogenic thickness of a plate (e.g., Maggi et al., 2000; Jackson, 2002; Burov, 2011; Molnar, 2020), the results of our analysis can additionally contribute to understand the dynamics of the geological features, identifying their deformation conditions, induced by tectonic stresses. Given the correlation between the depth to the BDT and permeability of rocks, our results can also help plan the explorative studies for high enthalpy geothermal systems, which would support a sustainable energy development. To this purpose, we should consider that in geothermal areas the BDT is expected to be at shallow depth levels. For instance, in Iceland (Reykjanes, Hengill, and Krafla) temperatures are in a range of 400–600 °C at a depth < 5 km and thus the BDT occurs close to the surface (e.g., Elders et al., 2014; Friðleifsson et al., 2014; Scott et al., 2015). In this case, the *S*-wave can be measured with less uncertainties and thus also small Q_s variations could be detected. A shallow BDT depth favours a fast strength decrease below it and sharp Q_s reduction, both making the transition zone to a ductile deformation thin and more easily detectable. In some volcanic areas (e.g., the Campi Flegrei), the strain rate can be significantly higher than those assumed in our study, reaching values up to 10^{-8} s^{-1} (Castaldo et al., 2018). This would partially counteract the effect of temperature, favoring the thickening of the brittle layer, but, at the same time, strongly enhance the Q_s reduction at the BDT depth and below it. Therefore, our approach for detecting the BDT depth and ductile crustal conditions is particularly suitable for geothermal areas. Measurements of variations in the Q_s, together with a knowledge of the active tectonics, rheological and thermal conditions of these areas, can help select suitable locations for deep drilling, to exploit supercritical hydrous fluids and define abundance, location, and size of geothermal resources.

In this regard, it is worth mentioning that the transition from brittle to ductile deformation, can occur through other mechanisms than dislocation creep, including diffusion creep, pressure solution,

Table 3
Determination coefficient (R^2) of a third order polynomial function ($y = p_0 + p_1x + p_2x^2 + p_3x^3$), fitting Q_s values with respect to temperature, for each value of the assumed strain rate.

	10^{-13} s^{-1} Strain rate					10^{-15} s^{-1} strain rate					10^{-17} s^{-1} strain rate				
Rheology	R^2	p_3	p_2	p_1	p_0	R^2	p_3	p_2	p_1	p_0	R^2	p_3	p_2	p_1	p_0
Dry Granite	0.99	$-2.566E^{-14}$	$1.677E^{-11}$	$-3.1E^{-09}$	244	0.99	$-1.036E^{-15}$	$6.771E^{-13}$	$-1.252E^{-10}$	244	0.99	$-4.183E^{-17}$	$2.734E^{-14}$	$-5.06E^{-12}$	244
Dry Quartzite	0.99	$-5.455E^{-14}$	$3.099E^{-11}$	$-5.161E^{-09}$	244	0.99	$-2.965E^{-15}$	$1.685E^{-12}$	$-2.806E^{-10}$	244	0.99	$-1.612E^{-16}$	$9.158E^{-14}$	$-1.526E^{-11}$	244
Dry Diabase	0.97	$-2.947E^{-14}$	$2.394E^{-11}$	$-5.226E^{-09}$	244	0.98	$-1.334E^{-15}$	$1.083E^{-12}$	$-2.365E^{-10}$	244	0.98	$-6.037E^{-17}$	$4.903E^{-14}$	$-1.07E^{-11}$	244
Dry OPX	0.95	$-3.26E^{-14}$	$2.817E^{-11}$	$-6.466E^{-09}$	244	0.95	$-2.221E^{-15}$	$1.919E^{-12}$	$-4.405E^{-10}$	244	0.95	$-1.513E^{-16}$	$1.307E^{-13}$	$-3.001E^{-11}$	244
Dry CPX	0.99	$-1.885E^{-15}$	$1.416E^{-12}$	$-2.906E^{-10}$	244	0.99	$-4.494E^{-17}$	$3.374E^{-14}$	$-6.927E^{-12}$	244	0.99	$-1.08E^{-18}$	$8.013E^{-16}$	$-1.605E^{-13}$	244
Wet Granite	0.99	$-1.967E^{-12}$	$1.496E^{-09}$	$-3.102E^{-07}$	244	0.99	$-2.22E^{-13}$	$1.689E^{-10}$	$-3.502E^{-08}$	244	0.99	$-2.506E^{-14}$	$1.907E^{-11}$	$-3.953E^{-09}$	244
Wet Quartzite	0.98	$-4.268E^{-12}$	$3.47E^{-09}$	$-7.582E^{-07}$	244	0.98	$-4.818E^{-13}$	$3.918E^{-10}$	$-8.559E^{-08}$	244	0.98	$-5.439E^{-14}$	$4.422E^{-11}$	$-9.662E^{-09}$	244

cataclastic flow, twinning, to name a few. This said, the observed reduction in the Q_s, associated to the onset of ductile conditions, can be masked by the effect of microfracturation, usually characterized by other deformation mechanisms. For instance, twinning, responsible for the initial yield in carbonates, is accompanied by pronounced microcraking, depending on the applied temperature, pressure, stress, and strain rate (e.g., Frederich et al., 1989; Meyer et al., 2019; Noël et al., 2021 Rybaki, 2021). We should further consider that fracturing causes an increase in the bulk permeability, favoring the influx of fluids, and precipitation of minerals (e.g., phyllosilicate), having a much weaker rheology than the rock's matrix (e.g., Collettini et al., 2019). Therefore, the BDT should rather identify a broader zone of finite thickness, in which both frictional and viscous deformation mechanisms are active, rather than a specific depth level (e.g., Meyer et al., 2019; Fagereng and Beall, 2021). The transition from brittle to ductile deformation is gradual also considering that rocks are polycrystalline materials, with each crystal having its onset of plastic deformation occurring under different conditions (Noël et al., 2021). In this transition zone, where slow slip events and tremors can nucleate (e.g., Fagereng et al., 2014), the rock deforms in a semi-brittle regime and we can expect a variation in the seismic attenuation, which would reflect the superimposed effects of fracturation, fluids, and composite rock's rheologies, and not only the effect of the incipient ductile deformation.

This study represents a first attempt to provide a general correlation between viscous rock's deformation and their seismic attenuation and quantify the reduction of the Q_s specific of a transition to a ductile deformation mode, as well as of a fully ductile deformation, despite the complexity of the rocks rheology. We expect that in the near future lab experiments and seismic measurements in the field can add further constraints on the results of this study.

5. Conclusions

In this study, we computed the shear seismic attenuation ($1/Q_s$), according to the Burgers and Gassmann mechanical model, using as input seven crustal rocks rheologies, two in hydrated and five in anhydrous conditions, different strain rates (10^{-13}, 10^{-15}, 10^{-17} s^{-1}, respectively) and thermal conditions ('*hot*' and '*cold*', respectively, representative of the cratonic and tectonically active areas conditions). We analysed variations in the Q_s with depth, in relation with mode of rock's deformation, derived from the corresponding yield strength envelopes.

The obtained results allowed us to quantify the orders of magnitude in the viscosity (η_s) and reduction of Q_s with respect its surface value, characterizing the average depth of the transition from brittle to ductile deformation (BDT) for each strength envelope. We observed that the amount of the η_s and Q_s reduction at the BDT depth strongly depends on the strain rate and is less affected by the chosen rheology and temperature conditions. These two last parameters exert a great influence on the computed Q_s reduction, when the rocks deform in fully ductile conditions. We also noticed that the reduction in Q_s at the depth of the BDT has a fixed order of magnitude, which proportionally increases with the input strain rate (10^{-12}, 10^{-10}, and 10^{-8}% for 10^{-17}, 10^{-15}, and 10^{-13} s^{-1}, respectively). In contrast, at the same depth, the η_s displays an opposite trend and varies up to one order of magnitude, under the same strain rate, but changing thermal conditions and rheology. Below the BDT depth, at the assumed base of the crust (40 km), the η_s and Q_s reduction decreases and increases by several orders of magnitude (up to four), showing the lowest (10^{17} Pa s) and highest (10^{-4}%) values, respectively, for the greatest strain rate, hottest geotherm, and hydrous rheologies. Furthermore, the analysis of the Q_s variations as a function of temperature revealed that the best fit is given by polynomial functions of the same order, mainly depending on the rock's rheology. This supports the validity of our results for a wide range of rheological types and tectonic settings.

We finally discussed how the determination of Q_s, as described in this

study, can be useful to map the extent of the BDT depth in tectonically active areas, despite the uncertainties affecting the lab rheological experiments and field data. In addition, Q_s can also be considered as a complementary proxy for the assessment of drilling operations in high enthalpy geothermal reservoirs, characterized by high temperatures, and thus preferentially deforming in ductile conditions, at shallow depth levels. In contrast, our results are less applicable to cratonic areas, which are usually composed of stiff crustal rheologies and exhibit low temperature and strain rate, all conditions that prevent a significant Q_s decrease with depth (i.e. seismic attenuation increase).

Declaration of Competing Interest

The authors declare that they have no known competing financial interests or personal relationships that could have appeared to influence the work reported in this paper.

Data availability

Data will be made available on request.

Acknowledgements

This study is supported by the PhD grant of M.A. Natale Castillo (DOTTMIUR36-NATALE-CASTILLO). Valuable comments of Luca De Siena, Nobuaki Fuji, and an anonymous reviewer, greatly improved the original manuscript.

Appendix A. Appendix

Table A1
Name of the variables used in this study with their units and range of values.

Variable	Parameter	SI	Range
Pre-exponential factor	A_{PL}	$Pa^{-N}s^{-1}$	$1.58E^{-37}$ - $1.26E^{-13}$
Activation energy	E_{PL}	J/mol	134,000–380,000
Exponential factor	N	–	1.9–5.3
Solid density	ρ_s	kg/m^3	2672.8–3277
Dry shear modulus	μ_0	GPa	37–75
Depth	z	km	0–40
Gravity acceleration	g	m/s^2	9.81
Temperature	T	°C	0–732.49
Pressure dependent constant for granular material	a_2	–	0.48
Pressure dependent constant for granular material	p_2	–	55.55
Pore pressure	p_0	Pa	0.36* p_c *(confining pressure)*
Fluid (water) density	ρ_f	kg/m^3	1000
Fluid (air) density	ρ_f	kg/m^3	1.225
Porosity	ϕ	%	0.3
Shear velocity	V_s	m/s	3576.43–4857.00
Shear seismic quality factor	Q_s	–	244.04094–244.004098
Friction coefficient-stress field orientation	α	–	0.75–3
Friction-related differential stress	σ_b	MPa	87.15–3857.68
Pore fluid factor	λ	–	0.36
Shear viscosity	η_s	Pa s	10^{17}–10^{38}

References

Afonso, J.C., Ranalli, G., 2004. The reference is: Crustal and mantle strengths in continental lithosphere: is the jelly sandwich model obsolete? Tectonophysics 394, 221–232.

Artemieva, I.M., 2006. Global 1°×1° thermal model TC1 for the continental lithosphere: implications for lithosphere secular evolution. Tectonophysics 416, 245–277.

Bourbiè, T., Coussy, O., Zinszner, B., 1987. Acoustics of Porous Media. Technip, Paris.

Burgmann, R., Dresen, G., 2008. Rheology of the lower crust and upper mantle: evidence from rock mechanics, geodesy, and field observations. Annu. Rev. Earth Planet. Sci. 36, 531–567.

Burov, E.B., 2011. Rheology and strength of the lithosphere. Mar. Pet. Geol. 28, 1402–1443.

Byerlee, J., 1978. Friction of Rocks. In: Byerlee, J.D., Wyss, M. (Eds.), Rock Friction and Earthquake Prediction. Contributions to Current Research in Geophysics (CCRG), vol. 6. https://doi.org/10.1007/978-3-0348-7182-2_4. Birkhäuser, Basel.

Cammarano, F., Goes, S., Vacher, P., Giardini, D., 2003. Inferring upper-mantle temperatures from seismic velocities. Phys. Earth Planet. Inter. 139, 197–222.

Carcione, J.M., 2014. Wave Fields in Real Media (Third Edition). Elsevier.

Carcione, J.M., Poletto, F., 2013. Seismic rheological model and reflection coefficients of the brittle–ductile transition. Pure Appl. Geophys. 170, 12. https://doi.org/10.1007/s00024-013-0643-4.

Carcione, J.M., Poletto, F., Farina, B., Craglietto, A., 2014. Simulation of seismic waves at the Earth crust (brittle–ductile transition) based on the Burgers model. Solid Earth 5, 1001–1010.

Carter, N.L., Tsenn, M.C., 1987. Flow properties of continental lithosphere. Tectonophysics 136, 27–63.

Castaldo, R., D'Auria, L., Pepe, S., Solaro, G., De Novellis, V., Tizzani, P., 2018. The impact of crustal rheology on natural seismicity: Campi Flegrei caldera case study. Geosci. Front. 10 (2), 453–466. https://doi.org/10.1016/j.gsf.2018.02.003.

Castro, R.R., Gallipoli, M.R., Mucciarelli, M., 2008. Crustal Q in Southern Italy determined from regional earthquakes. Tectonophysics 457, 1–2, 2008, 96–101, ISSN 0040-1951. https://doi.org/10.1016/j.tecto.2008.05.022.

Cermak, V., Bodri, L., Rybach, L., Buntebarth, G., 1990. Relationship between seismic velocity and heat production: comparison of two sets of data and test of validity. Earth Planet. Sci. Lett. 99 (1–2), 48–57.

Christensen, N.I., Mooney, W.D., 1995. Seismic velocity structure and composition of the continental crust: a global view. J. Geophys. Res. 100, 9761–9788. https://doi.org/10.1029/95JB00259.

Collettini, C., Tesei, T., Scuderi, M.M., Carpenter, B.M., Viti, C., 2019. Beyond Byerlee friction, weak faults and implications for slip behavior. Earth Planet. Sci. Lett. 519, 245–263.

Cooper, R.F., 2002. Seismic wave attenuation: energy dissipation in viscoelastic crystalline solids, 51 (1), 253–290. https://doi.org/10.2138/gsrmg.51.1.253.

Driesner, T., Geiger, S., 2007. Numerical simulation of multiphase fluid flow in hydrothermal systems. Rev. Mineral. Geochem. 65, 187–212.

Elders, W.A., Friðleifsson, G.Ó., Albertsson, A., 2014. Drilling into magma and the implications of the Iceland Deep Drilling Project (IDDP) for high-temperature geothermal systems worldwide. Geothermics 49, 111–118. ISSN 0375-6505,. https://doi.org/10.1016/j.geothermics.2013.05.001.

Fagereng, A., Beall, A., 2021. Complex fault zone behaviour a reflection of rheological heterogeneity? Phil. Trans. R. Soc. A 379, 20190421.

Fagereng, A.W.B., Hillary, G.W.B., Diener, J.F.A., 2014. Brittle-viscous deformation, slow slip, and tremor. Geophys. Res. Lett. 41 (12), 4159–4167. https://doi.org/10.1002/2014GL060433.

Farina, B., Poletto, F., Mendrinos, D., Carcione, J.M., Karytsas, C., 2019. Seismic properties in conductive and convective hot and super-hot geothermal systems. Geothermics 82, 16–33. https://doi.org/10.1016/j.geothermics.2019.05.005.

Fernandez, M., Ranalli, G., 1997. The role of rheology in extensional basin formation modelling. Tectonophysics 282, 129–145.

Findley, W.N., Lai, J.S., Onaran, K., 1976. Creep and Relaxation of Nonlinear Viscoelastic Materials. Dover Publications, INC, 1989 New York.

Frederich, J.T., Evans, B., Wong, T-F., 1989. Micromechanics of the Brittle to Plastic Transition in Carrara Marble. J. Geophys. Res. 94 (B4), 4129–4145.
Friðleifsson, G.Ó., Elders, Wilfred, Albertsson, A., 2014. The concept of the Iceland Deep Drilling Project. Geothermics 49, 2–8. https://doi.org/10.1016/j.geothermics.2013.03.004.
Gerya, Taras, 2019. Introduction to Numerical Geodynamic Modelling. https://doi.org/10.1017/9781316534243.
Goes, S., Hasterok, D., Schutt, D.L., Klöcking, M., 2020. Continental lithospheric temperatures: A review. Phys. Earth Planet. Inter. 306, 106509.
Goetze, C., Evans, B., 1979. Stress and temperature in the bending lithosphere as constrained by experimental rock mechanics. Geophys. J. R. Astron. Soc. 59, 463–478. https://doi.org/10.1111/j.1365-246X.1979.tb02567.x.
Hasterok, D., Chapman, D., 2011. Heat production and geotherms for the continental lithosphere. Earth Planet. Sci. Lett. 307, 59–70. https://doi.org/10.1016/j.epsl.2011.04.034.
Jackson, J., 2002. Strength of the continental lithosphere: time to abandon the jelly sandwich? GSA Today 12(9).
Jackson, I., Faul, U.H., 2010. Grainsize-sensitive viscoelastic relaxation in olivine: Towards a robust laboratory-based model for seismological application. Phys. Earth Planet. Inter. 183 (1–2), 151–163.
Jacquey, A., Cacace, M., 2020. Multiphysics modeling of a brittle-ductile lithosphere part II -semi-brittle, semi-ductile deformation and damage rheology. J. Geophys. Res. 125 https://doi.org/10.1029/2019JB018475.
Jaya, M.S., Shapiro, S.A., Kristinsdóttir, L.H., Bruhn, D., Milsch, H., Spangenberg, E., 2010. Temperature dependence of seismic properties in geothermal rocks at reservoir conditions. Geothermics 39 (1), 115–123.
Karato, S.I., 1993. Importance of anelasticity in the interpretation of seismic tomography. Geophys. Res. Lett. 20, 1623–1626.
Karato, S., 2008. Deformation of Earth Materials: An Introduction to the Rheology of Solid Earth. Cambridge University Press, Cambridge. https://doi.org/10.1017/CBO9780511804892.
Karato, S., Spetzler, H.A., 1990. Defect microdynamics in mineralsand solid-state mechanisms of seismic wave attenuation and velocitydispersion in the mantle. Rev. Geophys. 28, 399–421.
Kaselow, A., Shapiro, S.A., 2004. Stress sensitivity of elastic moduli and electrical resistivity in porous rocks. J. Geophys. Eng. 1 (1), 1–11. https://doi.org/10.1088/1742-2132/1/1/001.
Kreemer, C., Blewitt, G., Klein, E.C., 2014. A geodetic plate motion and global strain rate model. Geochem. Geophys. Geosyst. 15, 3849–3889. https://doi.org/10.1002/2014GC005407.
Kristinsdóttir, L.H., Flóvenz, Ó., Árnason, K., Bruhn, D., Milsch, H., Spangenberg, E., Kulenkampff, J., 2010. Electrical conductivity and P-wave velocity in rock samples from high-temperature Icelandic geothermal fields. Geothermics 39 (1), 94–105.
Maggi, A., Jackson, J.A., Priestley, K., Baker, C., 2000. A re-assessment of focal depth distributions in southern Iran, the Tien Shan and northern India: do earthquakes occur in the continental mantle? Geophys. J. Int. 143, 629e661.
Mareschal, J.-C., Jaupart, C., 2004. Variations of surface heat flow and lithospheric thermal structure beneath the North American craton. Earth Planet. Sci. Lett. 223, 65–77.
Mareschal, J.-C., Jaupart, C., 2013. Radiogenic heat production, thermal regime and evolution of continental crust. Tectonophysics 609, 524–534.
Mavko, G., Mukerji, T., Dvorkin, J., 2010. The Rock Physics Handbook 437–478. Cambridge and University Press. https://doi.org/10.1017/CBO9780511626753.011.
Meyer, G.G., Brantut, N., Mitchell, M., T.M., Meredith, P.G., 2019. Fault reactivation and strain partitioning across the brittle-ductile transition. Geology 47 (12), 1127–1130. https://doi.org/10.1130/G46516.1.
Molnar, P., 2020. The brittle-plastic transition, earthquakes, temperatures, and strain rates. J. Geophys. Res. Solid Earth 125 (7), e2019JB019335 doi:ARTN e2019JB019335 10.1029/2019JB019335.
Noël, C., Passelègue, F.X., Violay, M., 2021. Brittle faulting of ductile rock induced by pore fluid pressure build-up. J. Geophys. Res. 126, e2020JB021331 https://doi.org/10.1029/2020JB021331.
Norton, D., Knight, J., 1977. Transport phenomena in hydrothermal systems: cooling plutons. Am. J. Sci. 277, 937–981.
Poletto, F., Farina, B., Carcione, J.M., 2018. Sensitivity of seismic properties to temperature variations in a geothermal reservoir. Geothermics 76, 149–163.
Ranalli, G., Murphy, D.C., 1987. Rheological stratification of the lithosphere. Tectonophysics 132 (4), 281–295. https://doi.org/10.1016/0040-1951(87)90348-9.
Rybaki, E., 2021. Semi-brittle deformation of Carrara marble: Hardening and twinning induced plasticity. J. Geophys. Res. Solid Earth 126, e2021JB022573. https://doi.org/10.1029/2021JB022573.
Sato, H., Fehler, M.C., Maeda, T., 2012. Seismic Wave Propagation and Scattering in the Heterogeneous Earth, Second edition. Springer, New York, USA.
Scott, S., Driesner, T., Weis, P., 2015. Geologic controls on supercritical geothermal resources above magmatic intrusions. Nat. Commun. 6, 7837. https://doi.org/10.1038/ncomms8837.
Sibson, R.H., 1974. Frictional constraints on thrust, wrench and normal faults. Nature 249, 542–544.
Tesauro, M., Kaban, M.K., Mooney, W.D., 2015. Variations of the lithospheric strength and elastic thickness in North America. Geochem. Geophys. Geosyst. 16 https://doi.org/10.1002/2015GC005937.
Turcotte, D.L., Schubert, G., 2014. Geodynamics. Cambridge University, p. 636.
Vinciguerra, S., Trovato, C., Meredith, P.G., Benson, P.M., Troise, C., Natale, 2006. Understanding the seismic velocity structure of Campi Flegrei Caldera (Italy): from the laboratory to the field case. Pure Appl. Geophys. 163, 2205–2221.
Violay, M., Heap, M.J., Acosta, M., et al., 2017. Porosity evolution at the brittle-ductile transition in the continental crust: Implications for deep hydro-geothermal circulation. Sci. Rep. 7, 7705. https://doi.org/10.1038/s41598-017-08108-5.
Watanabe, N., Numakura, T., Sakaguchi, K. Hanae, Saishu, H., Okamoto, A.E., Ingebritsen, S.E., Tsuchiya, N., 2017. Potentially exploitable supercritical geothermal resources in the ductile crust. Nat. Geosci. 10, 140–144. https://doi.org/10.1038/ngeo2879.
Wilks, K.R., Carter, N.L., 1990. Rheology of some continental lower crustal rocks. Tectonophysics 182, 57–77.
Zoback, M.L., Mooney, W.D., 2003. Lithospheric buoyancy and continental intraplate stress. Int. Geol. Rev. 45, 95–118.